Line Tension Effects for Liquid Droplets on Circular Surface Domains

Pedro Blecua, Reinhard Lipowsky, and Jan Kierfeld*

Max Planck Institute of Colloids and Interfaces, Science Park Golm, 14424 Potsdam, Germany

Received April 11, 2006. In Final Form: September 14, 2006

We study the morphologies of single liquid droplets wetting a substrate in the presence of the line tension of the three-phase contact line. On a homogeneous substrate, the line tension leads to a discontinuous unbinding of the droplet if its volume is decreased below a critical value. For a droplet wetting a structured surface with a circular domain, a *line tension contrast* gives rise to discontinuous depinning transitions of the contact line from the domain boundary as the droplet volume is varied. We calculate the corresponding free energy bifurcation diagram analytically for axisymmetric droplet shapes. Numerical minimization of the droplet free energy shows that line tension contrasts can stabilize nonaxisymmetric droplet shapes, thus modifying the bifurcation diagram. These latter shapes should be accessible to experiments and can be used to reveal the presence of a line tension contrast.

1. Introduction

The morphology of liquid droplets on chemically or topographically structured substrates is determined by the interplay of the interfacial free energies of the droplet and the wettability pattern on the substrate for droplets in the millimeter and micrometer regime. This interplay can give rise to morphological transitions upon changing the volume V_β of the droplet or the wettability contrast and thus the contact angle of the substrate.[1,2] Experimentally, techniques such as microcontact printing[3] or monolayer lithography[4] allow the fabrication of imprinted or structured planar surfaces with tailored patterns of lyophilic and lyophobic surface domains. Morphological transitions of single droplets have been theoretically and experimentally studied for a variety of wettability patterns such as lyophilic circles on a lyophobic substrate,[5] lyophilic and lyophobic stripes,[6−9] and lyophilic rings on a lyophobic background.[10] Morphological transitions take place if the droplet volume V_β becomes comparable or bigger than a reference volume defined by the surface domain. Within this regime of droplet volumes, the morphology can change by exploiting the variability of the contact angle at the boundary of a surface domain.[2]

With decreasing droplet size, the line tension free energy contribution (i.e., the excess free energy arising from the three phase contact line[11]) becomes increasingly important. Line tension effects can no longer be neglected for droplets with a linear size below 100 nanometers.[1,12,13] Experimentally, line tension effects have been observed for droplet sizes in the nanometer regime[14,15]

up to the micrometer regime.[16] For droplets wetting a homogeneous substrate, line tension effects have been theoretically studied in ref 17. It has been found that, in the presence of line tension, the droplet discontinuously unbinds from the substrate upon decreasing its volume below a critical value. In this paper, we want to focus on the line tension effects for patterned substrates. In general, chemical patterning of substrates will lead both to a wettability contrast and to a contrast of the line tension. Such line tension contrasts can strongly modify the morphological transitions of small droplets. In this article, we study the effect of a line tension contrast for a single droplet on a lyophilic circular domain embedded in a lyophobic substrate.[5] Even for this relatively simple system, the line tension contrast leads to a qualitative change in the depinning behavior of the droplet's contact line at the boundary of the circular domain. Whereas the depinning of the contact line at the circular domain boundary is continuous if line tension effects can be ignored,[5] it becomes *discontinuous* in the presence of a line tension contrast (see Figure 6). For axisymmetric droplet shapes, we can characterize the discontinuous depinning of the contact line analytically by analyzing the interfacial and line free energies as a function of the droplet volume V_β. Line tension contrasts can also give rise to stable nonaxisymmetric shapes, as shown in Figure 10 below, and thus to a spontaneous breaking of the axial symmetry of the system. Using numerical free energy minimization, we study how the analytical results for axisymmetric shapes are modified if nonaxisymmetric shapes are taken into account in the analysis.

The paper is organized as follows. In section 2, we present our geometric interface model for fluids wetting a structured substrate. In section 3, we briefly review the discontinuous unbinding transition of a droplet wetting a homogeneous substrate in the presence of line tension.[17] In section 4, we study effects from a spatially homogeneous line tension on the continuous depinning transition of a single droplet on a circular domain. In section 5, we present a detailed study of a single droplet on a circular domain in the presence of a line tension contrast, where the droplet exhibits discontinuous depinning transitions. In subsection 5.1, we present the main results, and, in subsection 5.2, we present an analytical study for a sharp line tension contrast.

* Corresponding author.

(1) Lipowsky, R.; Lenz, P.; Swain, P. *Colloids Surf., A* **2000**, *161*, 3.
(2) Lipowsky, R.; Brinkmann, M.; Dimova, R.; Haluska, C.; Kierfeld, J.; Shillcock, J. *J. Phys.: Condens. Matter* **2005**, *17*, S2885.
(3) Xia, Y.; Whitesides, G. M. *Angew. Chem., Int. Ed.* **1998**, *37*, 550.
(4) Burmeister, F.; Schäfle, C.; Matthes, T.; Böhmisch, M.; Boneberg, J.; Leiderer, P. *Langmuir* **1997**, *13*, 2983.
(5) Lenz, P.; Lipowsky, R. *Phys. Rev. Lett.* **1998**, *80*, 1920.
(6) Gau, H.; Herminghaus, S.; Lenz, P.; Lipowsky, R. *Science* **1999**, *283*, 46.
(7) Darhuber, A. A.; Troian, S. M.; Miller, S. M.; Wagner, S. *J. Appl. Phys.* **2000**, *87*, 7768.
(8) Brinkmann, M.; Lipowsky, R. *J. Appl. Phys.* **2002**, *92*, 4296.
(9) Klingner, A.; Mugele, F. *J. Appl. Phys.* **2004**, *95*, 2918.
(10) Lenz, P.; Fenzl, W.; Lipowsky, R. *Europhys. Lett.* **2001**, *53*, 618.
(11) Rowlinson, J. S.; Widom, B. *Molecular Theory of Capillarity*; Clarendon Press: Oxford, 1982.
(12) Swain, P.; Lipowsky, R. *Langmuir* **1998**, *14*, 6772.
(13) Brinkmann, M.; Kierfeld, J.; Lipowsky, R. *J. Phys. A: Math. Gen.* **2004**, *37*, 11547.
(14) Pompe, T.; Herminghaus, S. *Phys. Rev. Lett.* **2000**, *85*, 1930.

(15) Seemann, R.; Jacobs, K.; Blossey, R. *J. Phys.: Condens. Matter* **2001**, *13*, 4915.
(16) Duncan, D.; Li, D.; Gaydos, J.; Neumann, W. *J. Colloid Interface Sci.* **1995**, *169*, 256.
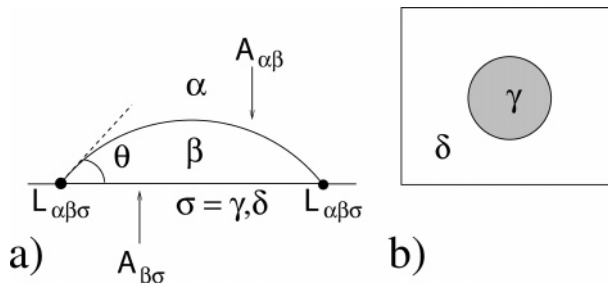(17) Widom, B. *J. Phys. Chem.* **1995**, *99*, 2803.

Figure 1. (a) Spherical droplet on a homogeneous substrate σ. (b) Circular lyophilic domain γ embedded in a lyophobic substrate δ.

In subsection 5.3, we investigate a continuous line tension contrast, and, in subsection 5.4, we study the effects from thermal fluctuations. In subsection 5.5, we analyze nonaxisymmetric droplet shapes numerically and discuss how they modify the depinning transitions. Finally, we discuss the experimental implications of our theory in section 6.

2. Model

2.1. Free Energy. We consider a single droplet of a liquid β that is deposited onto a solid substrate σ and surrounded by a vapor phase or another immiscible liquid phase α. We will study two simple generic substrate geometries: (i) a *homogeneous* substrate and (ii) a structured substrate containing a *single circular lyophilic domain* γ, which is embedded in a lyophobic substrate δ (see Figure 1).

Our analysis is based on the minimization of the interfacial and contact line free energies associated with the $\alpha\beta$ interface, which is represented by the mathematical surface $\mathscr{A}_{\alpha\beta}$ with area $A_{\alpha\beta} \equiv |\mathscr{A}_{\alpha\beta}|$. The droplet β wets a surface $\mathscr{A}_{\beta\sigma}$ on the substrate, which is bounded by the three phase contact line $\mathscr{L}_{\alpha\beta\sigma}$ (see Figure 1). On a chemically heterogeneous substrate, both surface tensions $\Sigma_{\alpha\sigma}(\mathbf{x})$ and $\Sigma_{\beta\sigma}(\mathbf{x})$ as well as the line tension $\Lambda(\mathbf{x})$ are functions of the position $\mathbf{x}$ on the substrate. The total free energy of the droplet on a chemically heterogeneous substrate assumes the form[8,12]

$$\mathscr{F} = \Sigma_{\alpha\beta}A_{\alpha\beta} + \int_{\mathscr{A}_{\beta\sigma}} dA[\Sigma_{\beta\sigma}(\mathbf{x}) - \Sigma_{\alpha\sigma}(\mathbf{x})] + \int_{\mathscr{L}_{\alpha\beta\sigma}} dL\Lambda(\mathbf{x}) + \Delta P V_{\beta} \quad (1)$$

where V_{β} is the volume of the droplet and ΔP is the Laplace pressure, defined as $\Delta P \equiv P_{\alpha} - P_{\beta}$. For a fixed volume V_{β}, the last term on the right-hand side of eq 1 plays the role of a Lagrange multiplier.[8]

For locally stable equilibrium morphologies, the first variation of the free energy (eq 1) with respect to small displacements of the $\alpha\beta$ interface and associated displacements of the three phase contact line $\mathscr{L}_{\alpha\beta\sigma}$ vanishes. Local equilibrium with respect to displacements of the $\alpha\beta$ interface leads to the Laplace equation

$$2M\Sigma_{\alpha\beta} = -\Delta P \quad (2)$$

where M is the mean curvature of the $\alpha\beta$ interface. According to the Laplace equation (eq 2) the droplet attains a shape of *constant mean curvature*.

For uniform substrate surfaces, the Young equation represents the condition of mechanical equilibrium of the three-phase contact line. This equation has to be generalized for nonvanishing line tension, as was first realized in ref 18 and extended to certain

(18) Gretz, R. D. *J. Chem. Phys.* **1966**, *45*, 3160.

surface domain geometries in refs 19 and 20. More recently, Swain and Lipowsky[12] derived a rather general contact line equation, which is valid for rigid substrates, both topographically and chemically structured, and stability criteria based on the second variation with respect to the contact line position were obtained in refs 13, 21, and 22. Local equilibrium with respect to displacements of the three phase contact line $\mathscr{L}_{\alpha\beta\sigma}$ leads to the generalized Young or contact line equation[12,13,21]

$$\Sigma_{\alpha\beta}\cos\theta = \Sigma_{\alpha\beta}w - \Lambda c_g^* - \hat{\mathbf{m}}\cdot\nabla^*\Lambda \quad (3)$$

where θ is the local contact angle and where we introduce the wettability

$$w(\mathbf{x}) \equiv \frac{\Sigma_{\alpha\sigma}(\mathbf{x}) - \Sigma_{\beta\sigma}(\mathbf{x})}{\Sigma_{\alpha\beta}} \quad (4)$$

which is the cosine of the contact angle θ_∞ of a *macroscopic* droplet, for which line tension effects can be ignored ($w = \cos\theta_\infty$). Furthermore, c_g^* is the geodesic curvature of $\mathscr{L}_{\alpha\beta\sigma}$ with respect to the substrate, ∇^* is the two-dimensional gradient on the substrate, and $\hat{\mathbf{m}}$ is a conormal perpendicular to both the surface $\mathscr{A}_{\beta\sigma}$ and the tangent to the three-phase contact line. In the following, we will focus on planar substrates, where $\hat{\mathbf{m}}$ equals the normal of the contact line $\mathscr{L}_{\alpha\beta\sigma}$, and c_g^* equals the curvature of $\mathscr{L}_{\alpha\beta\sigma}$.

In the following sections, we will study the effects of line tension on the equilibrium morphologies of a single droplet of fixed volume V_{β}. The equations of Laplace and Young describe *locally* stable configurations of the droplet. The Laplace equation (eq 2) is satisfied by shapes of constant mean curvature, which are *spherical caps* on a homogeneous substrate, with the contact line equation (eq 3) determining the contact angle and thus the radius of the spherical cap. Apart from homogeneous substrates, we also consider structured surfaces with *circular* domains, for which the contact line equation (eq 3) is also compatible with the spherical cap shape. For spherical caps, the wetted substrate surface, $\mathscr{A}_{\beta\sigma}$, is a circular domain of radius r, and the contact line equation (eq 3) becomes

$$\cos\theta = w - \frac{\Lambda}{\Sigma_{\alpha\beta}r} - \frac{\partial_r\Lambda}{\Sigma_{\alpha\beta}} \quad (5)$$

We will first constrain our local stability analysis to the subset of droplet shapes consisting of spherical caps. For this subset, we can obtain an analytical theory of the discontinuous unbinding transition on the homogeneous substrate, as in ref 17. Using the same subset of axisymmetric spherical cap shapes, we will also analytically treat the discontinuous depinning transitions arising from line tension effects for a circular lyophilic domain. In a second step, we will discuss how these results are modified if nonaxisymmetric shapes are included into the analysis. This will be done systematically using numerical minimization methods.

To find the *globally* stable state, we have to analyze all locally stable configurations and, furthermore, possible boundary minima. For a homogeneous substrate, the only relevant boundary minimum is a spherical droplet, which becomes unbound from the substrate, as shown in Figure 2. For a structured surface with a circular domain, additional minima arise for droplets whose

(19) Boruvka, L.; Neumann, A. W. *J. Chem. Phys.* **1977**, *66*, 5464.
(20) Rusanov, A. I. *Colloid J. USSR (Engl. Transl.)* **1977**, *39*, 618.
(21) Rosso, R.; Virga, E. G. *Phys. Rev. E* **2003**, *68*, 12601.
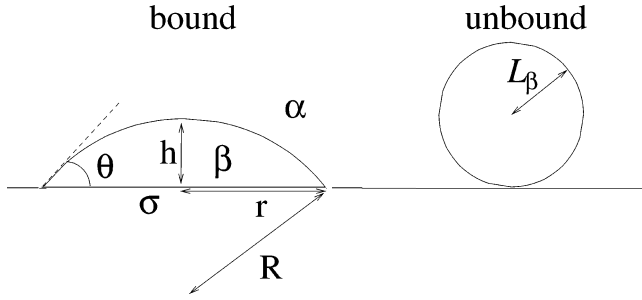(22) Rosso, R.; Virga, E. G. *J. Phys. A* **2004**, *37*, 3989.

Figure 2. Bound and unbound droplets.

circular contact line is *pinned* at the boundary of the circular lyophilic substrate domain γ.

2.2. Separation of Length Scales. Apart from the linear size $L_\beta \propto V_\beta^{1/3}$ of the droplet, which is determined by its volume V_β, the free energy of the droplet contains a number of different length scales associated with (i) gravity, (ii) molecular distances and interface widths, (iii) critical correlations of the wetting transition, and (iv) line tension.

In the expression (eq 1) for the droplet free energy, we neglected contributions arising from gravity. This is justified for droplet sizes L_β, which are much smaller than the capillary length ℓ_G, which is typically in the millimeter range.

On the other hand, the interfacial and contact line free energy model (1) is only applicable for droplet sizes L_β much larger than typical molecular distances ℓ_{mol}, and much larger than the interface width $\ell_{\alpha\beta}$ and the contact line width $\ell_{\alpha\beta\sigma}$. All of these microscopic length scales should be on the order of 1 nm.[1] We also assume that we have coexistence of the α and β phases, but that we are far away from a critical point, such that the correlation length ξ_β in the liquid phase is comparable to the molecular length l_{mol} and much smaller than the droplet length scale L_β. It is assumed as well that the temperature T of the system is below the wetting temperature T_w, that is, $T < T_w$.

Finally, we want to estimate the range of length scales where we expect line tension effects to become relevant. The line free energy contribution in eq 1 becomes comparable with the interfacial contribution for droplet sizes L_β below a characteristic length scale[1]

$$L_\beta^* = \frac{|\Lambda|}{\Sigma_{\alpha\beta}} \sim \frac{\ell_{\alpha\beta\gamma}^2}{\ell_{\alpha\beta}} \qquad (6)$$

where we used the estimates $|\Lambda| \sim (T/\ell_{mol}^3)\ell_{\alpha\beta\sigma}^2$ and $\Sigma_{\alpha\beta} \sim (T/\ell_{mol}^3)\ell_{\alpha\beta}$ (T is measured in energy units). For droplet sizes $L_\beta < L_\beta^*$, the line tension contribution to the free energy (eq 1) is dominating, and we expect pronounced line tension effects. Also, computer simulations on polymer melts demonstrate that the length scale L_β^* is comparable to a microscopic molecular length scale of the liquid.[23,24] For $L_\beta \gg L_\beta^*$, the line free energy is small compared to the interfacial contributions. In this regime, line tension effects are small but still observable. Line tension measurements based on the generalized Young equation (eq 3) are typically performed in this regime.[16]

The estimate $L_\beta^* \sim \ell_{\alpha\beta\gamma}^2/\ell_{\alpha\beta}$ in (eq 6) suggests that the regime $L_\beta < L_\beta^*$ is hardly accessible in experiments if the width of the contact line $\ell_{\alpha\beta\gamma}$ is small. The estimate for the line tension and thus $L_\beta^* = |\Lambda|/\Sigma_{\alpha\beta}$ can be substantially improved in the framework of an effective interface model[25] with an attractive

interface potential $U(l)$, which has a minimum at $l = l_{min}$ for partial wetting. Within the effective interface model, the potential depth $U_{min} = U(l_{min})$ is related to the (local) interfacial tensions by

$$|U_{min}| = \Sigma_{\alpha\beta} + \Sigma_{\beta\sigma} - \Sigma_{\alpha\sigma} = \Sigma_{\alpha\beta}(1 - \cos\theta) \qquad (7)$$

and the line tension can be calculated as[13,26]

$$\Lambda \approx (2\Sigma_{\alpha\beta})^{1/2}\left(\int_{l_{min}}^{l_{pin}} dl(U(l) + |U_{min}|)^{1/2} + \int_{l_{pin}}^{\infty} dl \frac{U(l)}{(U(l) + |U_{min}|)^{1/2}}\right) \qquad (8)$$

where l_{pin} is the inflection point of the effective interface potential $U(l)$.

Using the expression (eq 8) for short-range interface potentials with a range $l_{min} \sim l_{pin}$, we obtain an estimate

$$\Lambda \sim l_{min}(\Sigma_{\alpha\beta}|U_{min}|)^{1/2} \sim \Sigma_{\alpha\beta}l_{min}(1 - \cos\theta)^{1/2} \qquad (9)$$

If the wetting layer thickness l_{min} is comparable to the molecular size ℓ_{mol}, the length $L_\beta^* \sim \ell_{mol}$ is also comparable to the molecular length scale ℓ_{mol} such that, indeed, the regime $L_\beta < L_\beta^*$ is not experimentally accessible.

In the presence of long-range van der Waals forces, on the other hand, the effective interface potential has a tail $U(l) \approx A_H/12\pi l^2$ for large l, where A_H is the Hamaker constant.[27] Then we find[13]

$$\Lambda_{vdW} \approx \left(\frac{2\Sigma_{\alpha\beta}}{|U_{min}|}\right)^{1/2} \frac{A_H}{12\pi l_{pin}} \approx \frac{1}{6\pi\theta} \frac{A_H}{l_{pin}} \qquad (10)$$

where we used the small gradient expansion $|U_{min}| \approx \Sigma_{\alpha\beta}\theta^2/2$. For small contact angles θ or small wetting layer thicknesses l_{pin}, the line tension Λ_{vdW} and thus the corresponding length $L_\beta^* \sim A_H/\Sigma_{\alpha\beta}l_{pin}\theta$ becomes large. In this limit, the regime $L_\beta < L_\beta^*$ becomes experimentally accessible. On curved substrates, the line tension can also be controlled by varying the substrate curvature.[28,29]

Experimental values for $L_\beta^* = |\Lambda|/\Sigma_{\alpha\beta}$ range from tens of nanometers to tens of micrometers, reflecting the fact that line tension values in the range 10^{-11}J/m $\leq |\Lambda| \leq 10^{-6}$J/m have been reported.[14-16,30]

3. Homogeneous Substrates

We first review the analysis of equilibrium droplet shapes on *homogeneous* substrates with a spatially uniform wettability $w = \cos\theta_\infty$ and a spatially uniform line tension Λ. This case has been studied previously by Widom.[17] As already pointed out, we can limit our analysis to the subset of droplet shapes consisting of spherical caps, which represent surfaces of constant mean curvature satisfying the Laplace equation (eq 2). We consider a fixed droplet volume V_β, and we define the droplet size by

(23) Milchev, A. I.; Milchev, A. A. *Europhys. Lett.* **2001**, *56*, 695.
(24) Milchev, A.; Milchev, A.; Binder, K. *Comput. Phys. Commun.* **2002**, *146*, 38.
(25) Lipowsky, R. *Phys. Rev. Lett.* **1984**, *52*, 1429.

(26) Indekeu, J. O. *Physica A* **1992**, *183*, 439.
(27) Israelachvili, J. *Intermolecular and Surface Forces*; Academic Press: London, 1992.
(28) Marmur, A.; Krasovitski, B. *Langmuir* **2002**, *18*, 8919.
(29) Jakubczyk, P.; Napiórkowski, M. *Phys. Rev. E* **2005**, *72*, 11603.
(30) Gaydos, J.; Neumann, A. W. In *Applied Surface Thermodynamics*; Neumann, A. W., Spelt, J. K., Eds.; Marcel Dekker: New York, 1996.

$$L_\beta \equiv \left(\frac{3V_\beta}{4\pi}\right)^{1/3} \tag{11}$$

that is, as the radius of a sphere of volume V_β. For spherical caps, the wetted substrate surface $\mathscr{A}_{\beta\sigma}$ is a circle with radius r. For a fixed droplet volume, the radius r uniquely determines the shape of the spherical droplet. In *local* equilibrium, the radius r will be determined by the local minimum of the free energy (eq 1) as a function of r under the constraint of fixed volume V_β. The equilibrium value of r should fulfill the corresponding contact line equation (eq 5). Local equilibrium shapes represent *bound* droplets that partially wet the substrate (see Figure 2). The *global* equilibrium shape is given by the global minimum of the free energy, which can also be a boundary minimum. On a homogeneous substrate at a fixed volume V_β, the only possible boundary minimum is at $r = 0$, corresponding to a dewetting from the substrate, with the liquid β forming an *unbound* spherical droplet of radius L_β (see Figure 2). If the boundary minimum becomes the global minimum, the droplet unbinds from the substrate.[17]

For a spherical cap placed on the substrate such that the wetted surface $\mathscr{A}_{\beta\sigma}$ is a circle with radius r and area $A_{\beta\sigma} = \pi r^2$, the length of the three phase contact line is $L_{\alpha\beta\sigma} = 2\pi r$. The area of the surface $\mathscr{A}_{\alpha\beta}$ of the cap is $A_{\alpha\beta} = 2\pi r^2/(1 + \cos\theta) = \pi(r^2 + h^2)$, where h is the maximal height and θ is the contact angle of the spherical cap (see Figure 2). The geometry of a spherical cap is completely determined by specifying the two parameters h and r. For the following, it is convenient to introduce dimensionless quantities

$$f \equiv F/2\pi\Sigma_{\alpha\beta}L_\beta{}^2$$

$$\rho \equiv r/L_\beta$$

$$H \equiv h/r$$

$$\lambda_V \equiv \Lambda/\Sigma_{\alpha\beta}L_\beta \tag{12}$$

with the droplet size L_β defined in eq 11. The total dimensionless free energy f of the droplet assumes the form

$$f = \frac{1}{2}\rho^2(1 + H^2) - \frac{1}{2}w\rho^2 + \lambda_V\rho \tag{13}$$

where the wettability w and the dimensionless line tension λ_V are the remaining material parameters. The dimensionless line tension $|\lambda_V| = L_\beta^*/L_\beta \sim L_\beta^*/V_\beta^{1/3}$ is our control parameter for the droplet volume, which decreases with increasing volume. Because the wettability w is volume-independent, it follows from comparing free energy contributions in eq 13 that line tension effects become increasingly relevant at small volumes.

We want to consider the free energy (eq 13) for a fixed volume $V_\beta = \pi r^3(H^3 + 3H)/6$ of the spherical cap. The volume constraint thus gives a relation

$$\rho = 2(H^3 + 3H)^{-1/3} \tag{14}$$

between ρ and H, which can be inverted to obtain H as a function of ρ,

$$H = H(\rho) = g(4\rho^{-3}) \quad \text{with}$$

$$g(x) \equiv [x + (1 + x^2)^{1/2}]^{1/3} - [x + (1 + x^2)^{1/2}]^{-1/3} \tag{15}$$

We use the relation $H = H(\rho)$ in the free energy (eq 13) to explicitly include the volume constraint and obtain an expression

for the free energy $f = f(\rho)$ as a function of the dimensionless wetted radius ρ alone such that no Lagrange multiplier for the volume constraint is needed in the following. We now analyze f as a function of ρ in order to find the global free energy minimum, which can be either a local minimum fulfilling $\partial_\rho f(\rho_{bo}) = 0$ at a certain $\rho = \rho_{bo} > 0$ corresponding to a *bound* droplet or a possible boundary minimum at $\rho = \rho_{ub} = 0$ corresponding to an *unbound* droplet (see Figure 2).

To calculate the derivatives of $f(\rho)$ at constant volume V_β, we take derivatives with respect to ρ on both sides of eq 14, which gives

$$\partial_\rho H = -(H^3 + 3H)^{4/3}/2(1 + H^2) \tag{16}$$

This can be used to calculate

$$\partial_\rho f = \rho\frac{1 - H^2}{1 + H^2} - w\rho + \lambda_V \tag{17}$$

$$\partial_\rho^2 f = \frac{1 + 13H^2 + 3H^4 - H^6}{(1 + H^2)^3} - w \tag{18}$$

where $H = H(\rho)$ according to eq 15. Because

$$\cos\theta = \frac{1 - H^2}{1 + H^2} \tag{19}$$

for a spherical cap, we verify from eq 17 that the condition $\partial_\rho f(\rho_{bo}) = 0$ for a local minimum corresponding to a bound droplet is equivalent to the generalized Young equation (eq 5):

$$\cos\theta = w - \frac{\lambda_V}{\rho_{bo}} = w - \lambda_V\frac{(1 - \cos\theta)^{1/6}(2 + \cos\theta)^{1/3}}{2^{2/3}(1 + \cos\theta)^{1/2}} \tag{20}$$

The last line of eq 20 is an implicit equation for the contact angle θ of a bound droplet in terms of the wettability w and the dimensionless line tension λ_V (cf. ref 17), which we obtained by eliminating ρ_{bo} from eq 20 using the geometrical relation

$$\rho = \frac{2^{2/3}(1 + \cos\theta)^{1/2}}{(1 - \cos\theta)^{1/6}(2 + \cos\theta)^{1/3}} \tag{21}$$

which follows from eqs 14 and 19. Because $\lambda_V \sim \Lambda/\Sigma_{\alpha\beta}V_\beta^{1/3}$ is volume dependent according to eqs 12 and 11, the contact angle is also volume dependent in the presence of line tension.

Because $\partial_\rho f(0) = \lambda_V$, there is indeed a boundary minimum at $\rho = \rho_{ub} = 0$ for positive line tension, and the unbound droplet is locally stable. For negative or zero line tension, the unbound state becomes unstable, and the droplet is always in the bound state partially wetting the substrate.

For small positive line tension, the local minimum at $\rho = \rho_{bo} > 0$ corresponding to a bound droplet is the global minimum. Upon increasing the line tension to values $\lambda_V > \lambda_{V,ub}$ above an *unbinding threshold* $\lambda_{V,ub}$, the unbound state of the droplet with $\rho = \rho_{ub} = 0$ becomes the global minimum, and the droplet undergoes a *discontinuous unbinding transition*. The locus of the transition or unbinding line in parameter space is given by the generalized Young equation $\partial_\rho f(\rho_{bo}) = 0$, or eq 20, and the condition $f(\rho_{bo}) - f(0) = 0$ (where $f(0) = 2$). Using eqs 13 and 17 in these conditions, we can calculate an explicit parametrization of the unbinding line in the $\lambda_V - w$ plane in terms of the dimensionless height variable H:

$$\lambda_{V,ub}(H) = -\frac{2H(H^3 + 3H)^{2/3}}{1 + H^2} + 2(H^3 + 3H)^{1/3}$$

$$w_{ub}(H) = \frac{1 - 4H^2 - H^4}{1 + H^2} + (H^3 + 3H)^{2/3} \qquad (22)$$

The parameter $H = h/r$ runs from $H = 0$ (corresponding to cos $\theta = 1$ or complete wetting) to $H = \infty$ (corresponding to cos $\theta = -1$ or dewetting) for spherical caps. The resulting unbinding line is displayed in the morphological diagram of Figure 3.

Upon further increasing the line tension, the bound state becomes unstable for $\lambda_V > \lambda_{V,in}$ beyond an *instability threshold* $\lambda_{V,in}$. Within the regime $\lambda_{V,ub} < \lambda_V < \lambda_{V,in}$ of line tension, the bound state of the droplet remains metastable. The locus of the *instability line* is determined by the generalized Young equation $\partial_\rho f(\rho_{bo}) = 0$, or eq 20, and the additional condition $\partial_\rho^2 f(\rho_{bo}) = 0$. Using the results of eqs 17 and 18, we also obtain an explicit parametrization of the instability line in the λ_V–w plane:

$$\lambda_{V,in}(H) = \frac{8H}{(1 + H^2)^3(H^3 + 3H)^{2/3}}$$

$$w_{in}(H) = \frac{1 + 13H^2 + 3H^4 - H^6}{(1 + H^2)^3} \qquad (23)$$

which is also shown in the morphological diagram of Figure 3. In the λ_V–w plane, only the region $-1 \le w \le 1$ is physically accessible for bound droplets. At the boundary $w = 1$, the droplet completely wets the substrate, whereas it always unbinds from the substrate at $w = -1$, corresponding to dewetting.

Using the geometrical relation (eq 19) for cos θ, we can also readily obtain an explicit parametrization of the unbinding and instability line in the λ_V–θ plane in terms of H (see Figure 3), which has been obtained previously in a slightly different manner by Widom.[17] The condition $-1 \le w \le 1$ defines, together with the generalized Young equation $\partial_\rho f(\rho_{bo}) = 0$, or eq 20, a region in the λ_V–θ plane that is physically accessible for droplets and is also shown in the morphological diagram in Figure 3.

4. Circular Lyophilic Domains and Spatially Homogeneous Line Tension

In the remainder of the article, we focus on the effects of line tension on *depinning transitions* of the contact line of a *bound* droplet in the presence of wettability contrasts. We start with the analysis of the effect of a spatially uniform line tension Λ on droplet morphologies on a chemically patterned surface containing a *single circular lyophilic domain* γ with wettability $w_\gamma = \cos \theta_{\gamma,\infty}$ and radius a embedded in a lyophobic substrate δ with wettability $w_\delta = \cos \theta_{\delta,\infty} < w_\gamma$ (see Figures 1 and 4).

For a circular lyophilic domain with spatially homogeneous line tension, the droplet shapes of minimal energy are *spherical caps*, which are axisymmetrically placed on the circular domain. These shapes can be studied analytically. As in the previous section, we work at fixed droplet volume V_β, which is the basic control parameter in an experiment. Then the droplet shape is uniquely determined by the radius r of the contact area, or the dimensionless radius $\rho = r/L_\beta$ (see eq 12). The radius of the circular domain a (see Figure 4) introduces another length scale into the problem, and we define a dimensionless radius

$$\rho_V \equiv \frac{a}{L_\beta} = \left(\frac{4\pi a^3}{3V_\beta}\right)^{1/3} \qquad (24)$$

In the experiment, ρ_V is controlled by varying the volume V_β of
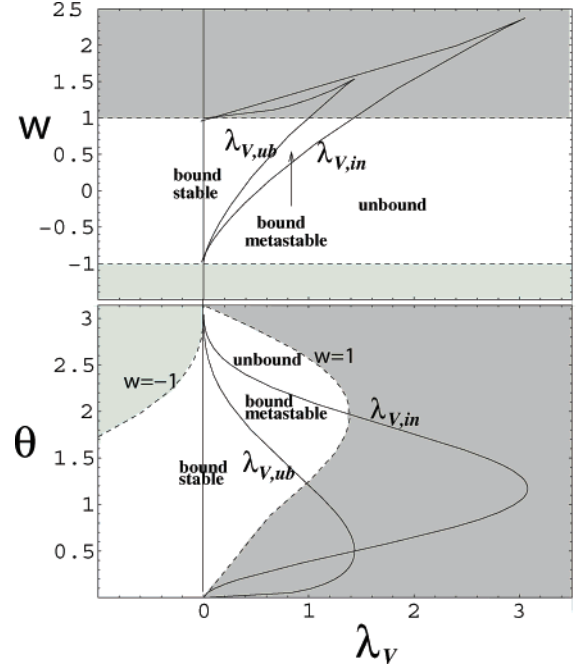
Figure 3. Morphological diagrams for a single droplet on a homogeneous substrate as a function of wettabilities w and dimensionless line tensions λ_V (top) and as a function of contact angles θ and dimensionless line tensions λ_V (bottom). $\lambda_{V,in}$ denotes the instability line and $\lambda_{V,ub}$ is the unbinding line, as given by eqs 22 and 23, respectively. For $\lambda_V < \lambda_{V,ub}$, the bound droplet is globally stable, for $\lambda_{V,ub} < \lambda_V < \lambda_{V,in}$ it becomes metastable, and for $\lambda_V > \lambda_{V,in}$ it becomes unstable. Only the unshaded region $-1 \le w \le 1$ in the w–λ_V plane is physically accessible for bound droplets; at $w = 1$, we find complete wetting, and, at $w = -1$, droplets always unbind. In the θ–λ_V plane, the condition $-1 \le w \le 1$ defines, together with the generalized Young equation (eq 20), a corresponding region of physically accessible states for bound droplets.
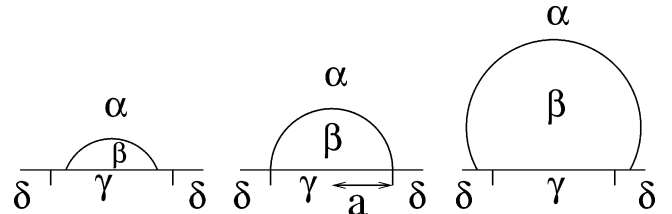
Figure 4. The three regimes of a single droplet in a circular lyophilic domain in a lyophobic matrix. From left to right, with increasing volume: regime I with $\theta = \theta_\gamma$, regime II with $\theta_\gamma < \theta < \theta_\delta$, and regime III with $\theta = \theta_\delta$.

the droplet, that is, by changing its size $L_\beta \sim V_\beta^{1/3}$ at fixed radius a of the surface domain.

The two other material parameters are the wettabilities and the dimensionless line tensions. By definition (eq 12), the dimensionless line tension is volume-dependent and, thus, acquires a dependence on ρ_V ($\lambda_V = \rho_V \Lambda/\Sigma_{\alpha\beta}a$) if the radius a is fixed. To display the full volume dependence of the free energy, it is advantageous to use the dimensionless and volume-independent line tension

$$\lambda \equiv \Lambda/\Sigma_{\alpha\beta}a = \lambda_V/\rho_V \qquad (25)$$

in the following.

Then, the dimensionless free energy f of a spherical cap-shaped droplet, which is axisymmetrically placed on the circular domain, assumes the compact and simple form

$$f = f_\gamma = \frac{1}{2}\rho^2[1 + H^2(\rho)] - \frac{1}{2}w_\gamma\rho^2 + \lambda\rho_V\rho \quad \text{for } \rho < \rho_V$$

$$f = f_\delta = \frac{1}{2}\rho^2[1 + H^2(\rho)] - \frac{1}{2}w_\delta\rho^2 + \lambda\rho_V\rho - $$
$$\frac{1}{2}\rho_V{}^2(w_\gamma - w_\delta) \quad \text{for } \rho > \rho_V \quad (26)$$
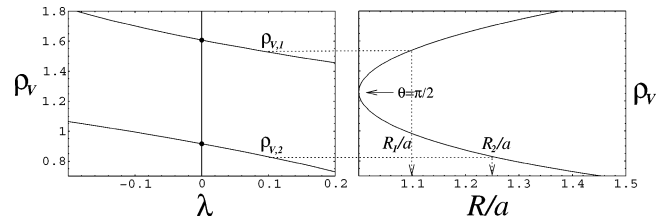

Figure 5. (left) The two dimensionless boundary domain sizes $\rho_{V,1}$ and $\rho_{V,2}$ (compare eq 24) as a function of the dimensionless line tension λ according to eqs 51 and 54. (right) The dimensionless boundary domain size as a function of the dimensionless curvature radius R/a of the droplet, which is given by a purely geometric relation. For each value of λ, we can read off the corresponding boundary domain sizes ($\rho_{V,1}$ and $\rho_{V,2}$) on the left and use them on the right to determine the corresponding range of observable curvature radii $R_1 < R < R_2$ for a pinned droplet.

where $H(\rho)$ is given by eq 15. For fixed wettabilities w_γ and w_δ and fixed line tension λ, the basic control parameter is the volume V_β, which enters into the equation through the dimensionless domain size ρ_V, as explained above. By minimizing this free energy with respect to ρ, for a given volume or given ρ_V, we obtain the equilibrium value of r, which, as mentioned, parametrizes the droplet's shape.

We present a detailed analysis of the free energy $f = f(\rho)$ as given by eq 26 in Appendix A. The main results of this analysis are presented in the following. For increasing volume, there are three regimes (I, II, III) of wetting behavior, which are illustrated in Figure 4. The wetting behavior is qualitatively similar to what was found in ref 5 for zero line tension.

In regime I, for small volumes V_β or large ρ_V, the droplet is entirely within the domain γ, and the contact angle is given by the generalized Young equation (eq 20) with the corresponding wettability $w = w_\gamma$, which describes the line tension effects on the contact angle. The generalized Young equation can be solved by using the additional geometrical relation (eq 21). This gives a weakly volume-dependent contact angle $\theta_\gamma = \theta_\gamma(\rho_V)$.

Analogously, in regime III, for large volumes V_β or small ρ_V, the droplet wets the surrounding substrate δ and completely covers the γ-domain. Then the contact angle is given by the generalized Young equation (eq 20) with the corresponding wettability $w = w_\delta$. Again, the generalized Young equation can be solved by using the additional geometrical relation (eq 21), which gives a weakly volume-dependent contact angle $\theta_\delta = \theta_\delta(\rho_V)$.

For intermediate volumes in regime II, the droplet gets pinned to the domain boundary. This creates a freedom of the contact angle, which will become strongly volume-dependent. Regime II occurs between two *boundary volumes*, $V_1 \leq V_\beta \leq V_2$, or $\rho_{V,1} \geq \rho_V \geq \rho_{V,2}$. These boundary values $\rho_{V,1}$ and $\rho_{V,2}$ are calculated explicitly in the appendix (see eqs 51 and 54). The corresponding *boundary contact angles* $\theta_{1,2}$ fulfill

$$\cos\theta_{1,2} = w_{\gamma,\delta} - \lambda \quad (27)$$

(see eqs 50 and 53 in Appendix A). The contact angle varies with the volume in the range $\theta_1 \leq \theta \leq \theta_2$ according to eq 19:

$$\cos\theta(\rho_V) = \frac{1 - H^2(\rho_V)}{1 + H^2(\rho_V)} \text{ for } \rho_{V,1} \geq \rho_V \geq \rho_{V,2} \quad (28)$$

At the transition from regimes I or III into regime II, the contact line becomes pinned, whereas it depins when it leaves regime II. We find that, for a lyophilic domain, both the pinning and depinning transition are *continuous* for a *homogeneous* line tension. This means that the equilibrium radius $\rho_{bo} = \rho_{bo}(\rho_V)$ of the bound droplet as a function of the volume changes *continuously* through the pinning and depinning transitions of the contact line at $\rho_V = \rho_{V,1}$ and $\rho_V = \rho_{V,2}$, respectively.

This wetting behavior is qualitatively similar to what was found in ref 5 for zero line tension, where analogous regimes exist. However, in the presence of line tension, the contact angles θ_γ and θ_δ in regimes I and III, respectively, are shifted with respect to the "macroscopic" angles $\theta_{\gamma,\infty} = \arccos w_\gamma$ and $\theta_{\delta,\infty}$

$= \arccos w_\delta$ due to the line tension corrections in the contact line equation (eq 20).

For comparison with experiments, it is instructive to see how relevant quantities describing the droplet's shape change in the presence of the (dimensionless) line tension λ. Because the volume V_β of a droplet or the corresponding parameter ρ_V (cf. eq 24) are the basic experimental control parameters, the boundary volumes $\rho_{V,1}$ and $\rho_{V,2}$ are two quantities that can be determined experimentally. The dependence of $\rho_{V,1}$ and $\rho_{V,2}$ on the line tension λ is given by eqs 51 and 54, derived in Appendix A. The left side of Figure 5 shows how $\rho_{V,1}$ and $\rho_{V,2}$ change as a function of the dimensionless line tension λ. Both $\rho_{V,1}$ and $\rho_{V,2}$ change approximately linearly for small positive and negative λ; for $\lambda > 0$, both quantities are reduced compared to $\lambda = 0$, and, for $\lambda < 0$, they are increased compared to $\lambda = 0$.

Another quantity that is measurable is the droplet's radius of curvature R (see Figure 2). For a pinned droplet, its radius of curvature R is related to its contact angle θ and its volume V_β by purely geometric relations. We insert $\cos\theta = \pm(1 - (R/a)^2)^{1/2}$ into the geometric relation (eq 21) with $\rho = \rho_V$ (for a pinned droplet with $r = a$) to obtain ρ_V as a function of the dimensionless radius of curvature R/a. This purely geometric relation is shown on the right side of Figure 5. For a given dimensionless line tension λ, we can now read off the range $\rho_{V,1} \geq \rho_V \geq \rho_{V,2}$ of pinned droplet volumes on the left-hand side of Figure 5 and determine the corresponding range of dimensionless curvature radii R_1/a and R_2/a using the right side of Figure 5. Because of the nonmonotonic behavior of R/a as a function of ρ_V with a minimum at $\rho_V = 2^{1/3} \simeq 1.26$ corresponding to a half sphere with $R/a = 1$, the lower boundary radius R_1 is decreased, while the upper boundary radius R_2 is increased if the line tension increases from zero to positive values. For negative line tension, the opposite happens.

5. Circular Lyophilic Domains and Line Tension Contrast

In the preceding sections, we studied effects from a *homogeneous* line tension on a single droplet wetting either a homogeneous substrate or a lyophilic circular domain γ embedded in a lyophobic substrate δ. By analyzing the interfacial and line free energies of the droplet, we found up to three distinct types of (meta)stable droplet morphologies. These shapes correspond to (i) unbound droplets for small volumes, as discussed in section 3, (ii) bound droplets inside the circular domain (regime I) or completely covering the γ-domain (regime III), and (iii) bound droplets with the contact line pinned at the domain boundary (regime II), as discussed in section 4. The two competing minima (ii) and (iii) give rise to the three morphological regimes I−III

for bound droplets, which are separated by *continuous* pinning and depinning transitions for a homogeneous line tension.

In the present section, we want to discuss, in detail, how these transitions are affected by the presence of a *line tension contrast* and, in particular, how the line tension contrast can give rise to discontinuous and hysteretic depinning transitions.

In general, chemical patterning not only leads to a wettability contrast with $w_\gamma > w_\delta$ for a lyophilic domain, but will also give rise to a *line tension contrast*. This can be easily understood in the framework of the effective interface model introduced in section 2.2: because of chemical patterning, the *depth* $U_{\min}$ of the interface potential and, according to eq 7, the wettability will vary across the domains. Also the *shape* of the interface potential and, therefore, according to eq 8, the line tension Λ will vary. Therefore, we study effects from a line tension contrast with different values $\Lambda_\gamma \neq \Lambda_\delta$ for the line tensions inside and outside the domain, respectively. In general, we can distinguish two cases: (i) For $\Lambda_\gamma < \Lambda_\delta$, the three-phase contact line prefers to run through the γ-domain because it offers a lower value of the line tension. Therefore, we will call the γ-domain "linophilic" in this case. (ii) For $\Lambda_\gamma > \Lambda_\delta$, the contact line prefers to avoid the γ-domain. Therefore, we will call the γ-domain "linophobic" in this latter case.

The change in line tension between the domain γ and the substrate δ changes over a characteristic width, which is comparable to the width of the contact line $\ell_{\alpha\beta\sigma}$. Regarding the spatial variation of the line tension, we can study two different cases: (i) In the limit of vanishing $\ell_{\alpha\beta\sigma}$, we can consider a *two-valued* line tension contrast, which exhibits a steplike behavior, as described by

$$\Lambda(r) = \Lambda_\gamma + \Theta(r - a)(\Lambda_\delta - \Lambda_\gamma) \qquad (29)$$

where $\Theta(x)$ is the Heaviside step function. (ii) In a more realistic model, we can also consider a *continuous* line tension contrast, as given by

$$\Lambda(r) = \frac{\Lambda_\delta - \Lambda_\gamma}{2}\tanh\left(\frac{r - a}{\ell_{\alpha\beta\sigma}}\right) + \frac{\Lambda_\delta + \Lambda_\gamma}{2} \qquad (30)$$

where the line tension changes continuously over the finite width $\ell_{\alpha\beta\sigma}$ across the $\gamma\delta$ boundary on the substrate. The qualitative results regarding the droplet depinning for a circular lyophilic domain will be the same for both steplike and continuous line tension contrasts.

5.1. Main Results. In this section, we will present our main results, which are summarized in the morphological diagrams in Figure 6 in the plane spanned by the two parameters $\Delta\lambda \equiv \lambda_\delta - \lambda_\gamma$, where λ_γ and λ_δ are the dimensionless volume-independent line tensions inside and outside of the domain, respectively, which are defined as in eq 25, and $\rho_V \sim V_\beta^{-1/3}$ is the dimensionless domain radius (eq 24) measuring the droplet volume. $\Delta\lambda > 0$ and $\Delta\lambda < 0$ correspond to the cases of a linophilic and linophobic domain, respectively. We postpone detailed derivations and discussions to the subsequent sections. In the previous section, we found *continuous* pinning and depinning transitions of the contact line for a lyophilic domain and a spatially homogeneous line tension $\Delta\lambda = 0$ both between the regimes I and II and between the regimes II and III. If we also include a line tension contrast (eq 29 or 30), we find for both the linophilic domain ($\Delta\lambda > 0$) and the linophobic domain ($\Delta\lambda < 0$) *discontinuous depinning transitions*, where the contact area of the droplet exhibits a discontinuity. For the linophilic case, the discontinuity occurs upon *increasing* the volume between regimes II and III. Then the contact line of a droplet on the γ-domain tends to
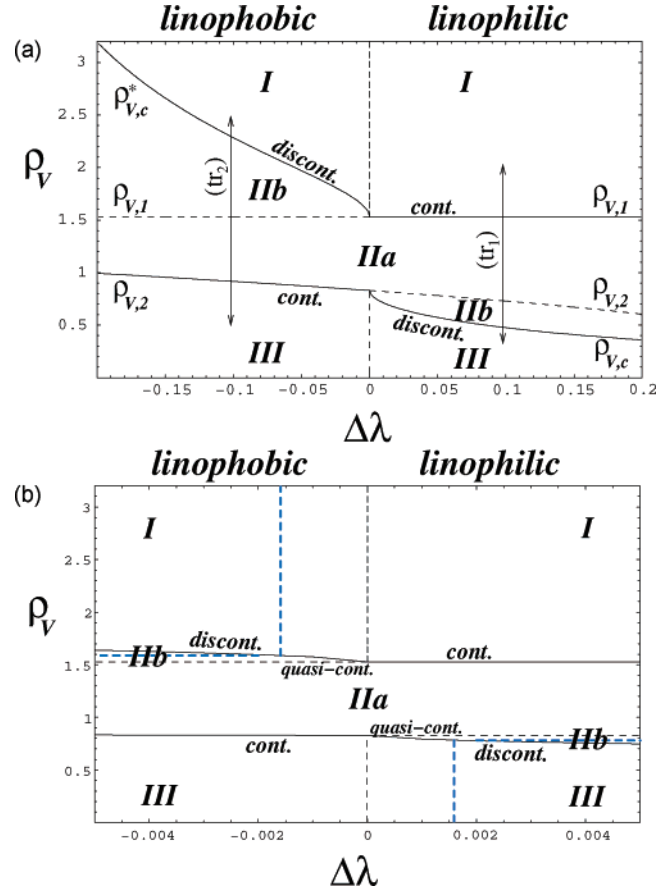

Figure 6. Morphological diagram as a function of the dimensionless line tension contrast $\Delta\lambda$ and the rescaled domain radius ρ_V, where $\Delta\lambda = \lambda_\delta - \lambda_\gamma$ with fixed $\lambda_\gamma = 0.1$, and for wettabilities $w_\gamma = 0.5$ and $w_\delta = -0.5$ in the absence (a) and presence (b) of thermal fluctuations. Pinning or depinning transitions are indicated by solid lines; dashed lines indicate instability lines, where metastable states become *mechanically unstable*. The free energy landscape along the trajectories (tr_1) and (tr_2) are shown in Figures 7 and 8, respectively. Blue dashed lines in the morphological diagram for nonzero temperature in panel b indicate instability lines, where the corresponding metastable states become *unstable with respect to thermal activation* for a domain radius $a = 10\ell_{\text{mol}}$. Effects from thermal fluctuations are small; therefore, we chose a smaller range of values $\Delta\lambda$ in panel b. In the region between the blue dashed vertical lines close to $\Delta\lambda = 0$, the system finds its minimum spontaneously, and the depinning transitions can be regarded as quasi-continuous.

adhere to the linophilic domain against the increasing interfacial energy of the $\alpha\beta$ interface of the growing droplet, and the droplet spreads onto the δ-substrate in a discontinuous depinning transition. For the linophobic case, the discontinuity occurs upon *decreasing* the volume between regimes II and I. Then the droplet initially wets the δ-substrate and covers the entire γ-domain. The shrinking contact line tends to avoid the linophobic γ-domain, although this stretches the $\alpha\beta$ interface, and the droplet pulls back onto the γ-substrate in a discontinuous depinning transition.

5.1.1. Axisymmetric Shapes. For axisymmetric shapes, that is, spherical droplets placed axisymmetrically on the circular domain, we can perform analytical calculations of the droplet morphologies based on the minimization its free energy $f = f(\rho)$ in order to find the equilibrium dimensionless contact radius ρ_{bo} of the droplet, analogously to the case of a homogeneous line tension in the previous section. The discontinuous depinning transitions show up as discontinuities $\Delta\rho_{\text{bo}}$ in the equilibrium radius of the droplet. This analysis finally leads to the morphological diagram Figure 6a in the absence of thermal fluctuations. The effects of thermal

fluctuations can be included into the analysis by taking into account that energy barriers with heights up to the order of T can be overcome by thermal activation and, thus, are effectively absent. This leads to modifications in the morphological diagram (see Figure 6b).

Our findings for zero temperature are summarized in the morphological diagram in Figure 6a. This morphological diagram is generic for the depinning behavior of *bound* droplets. If one of the line tensions becomes larger than the instability threshold $\lambda_{V,in}$ (i.e., $\lambda_\gamma \rho_V > \lambda_{V,in}(w_\gamma)$ or $\lambda_\delta \rho_V > \lambda_{V,in}(w_\delta)$; see section 3), the depinning transitions start to interfere with the unbinding transitions on the domain γ or the substrate δ. Then we expect a change in the general topology of the morphological diagram. In the present article, we do not consider this case. For both linophilic and linophobic domains, we find a strong hysteretic behavior at the discontinuous depinning transitions, which is also evident from the bifurcation diagrams in Figures 7 and 8 (blue curves), where we plot the global and metastable minima of the free energy as a function of the volume control parameter ρ_V.

Approaching the depinning transition between regimes II and III for a *linophilic domain* $\Delta\lambda > 0$ from small volumes (i.e., decreasing ρ_V), the pinned state of the droplet at the boundary minimum $\rho = \rho_V$ *never* becomes mechanically unstable in the absence of thermal fluctuations. In this metastable configuration, the droplet can exhibit very large contact angles. Another hallmark of the line tension contrast is the existence of a novel regime IIb, where metastable states also appear in regime II. For this range of volumes, the boundary minimum continues to be the global minimum because the contact line can gain energy by staying within the linophilic γ-domain, although a metastable minimum corresponding to a droplet sitting on the δ-substrate and completely covering the γ-domain already exists. The two minima exchange stability at a *critical value* $\rho_{V,c}$ corresponding to a critical volume V_c. Above this critical volume, it is energetically advantageous for the droplet to depin in a discontinuous transition with a discontinuity in the contact radius and wet the surrounding δ-matrix. Regimes IIb and III, where additional metastable states exist, are bounded by two instability lines where these metastable minima vanish and which are displayed as dashed lines in the morphological diagram in Figure 6. Because the pinned state $\rho = \rho_V$ does not become mechanically unstable for large volumes, regime III is bounded by a *vertical* instability line $\Delta\lambda = 0$.

The hysteresis behavior at the depinning transition between regimes I and II for a *linophobic domain* $\Delta\lambda < 0$ is analogous. Approaching the transition from large volumes (i.e., increasing ρ_V), the pinned state of the droplet at the boundary minimum $\rho = \rho_V$ *never* becomes mechanically unstable in the absence of thermal fluctuations. In this metastable droplet configuration, the droplet can exhibit very small contact angles. Again, there also exists a novel regime IIb, where the boundary minimum continues to be the global minimum, although a metastable minimum corresponding to a droplet sitting within the γ-domain already exists. The boundary minimum is stable because the contact line gains additional energy by staying outside the linophobic domain and on the surrounding δ-matrix. Only below the critical volume V_c^* corresponding to $\rho_{V,c}^*$, it is energetically favorable for the droplet to depin and retreat in a discontinuous transition with a discontinuity in the contact radius onto the linophobic γ-domain. Regime IIb and regime I, where additional metastable states exist, are again bounded by two instability lines (see Figure 6). Because the pinned state $\rho = \rho_V$ does not become mechanically unstable for large volumes, regime I is also bounded by a *vertical* instability line, $\Delta\lambda = 0$.
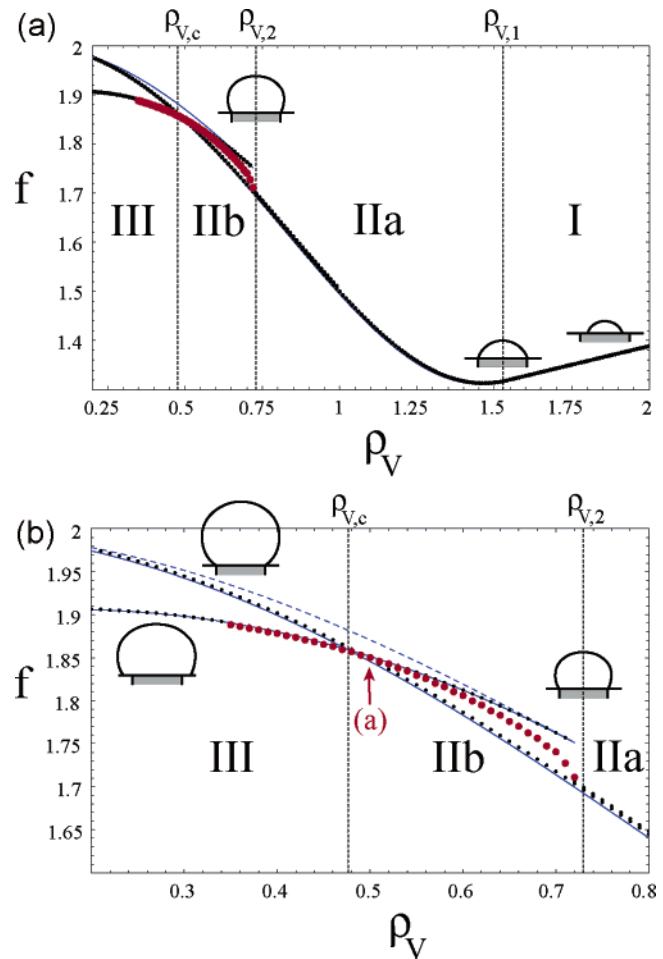

Figure 7. Linophilic domain. Free energy bifurcation diagram showing the global minima $f(\rho_{bo}) = f(\rho_{bo}(\rho_V))$ together with the branches of metastable minima as a function of the dimensionless domain radius ρ_V (see eq 24), for $w_\gamma = 0.5$, $w_\delta = -0.5$, and $\lambda_\gamma = 0.1$, $\lambda_\delta = 0.2$. The diagram in panel b is a close-up of the full diagram in panel a. Blue lines: Analytic results for axisymmetric shapes and steplike line tension contrast. We find $\rho_{V,c} \simeq 0.476$, $\rho_{V,1} \simeq 1.528$, and $\rho_{V,2} \simeq 0.729$. The regimes I, IIa, IIb, and III according to eq 63 are indicated. The pinning and depinning transition between regimes I and IIa is continuous, the depinning from regimes II to regime III is discontinuous, and the re-pinning from regime III to regimes II is continuous. The dashed blue line represents the branch of unstable free energy maxima. Black points: Results from numerical minimization restricted to axisymmetric shapes. Red points: Results from numerical minimization allowing for nonaxisymmetric shapes. The nonaxisymmetric shape in point a is shown in Figure 10a. Numerical results for continuous line tension and wettability contrasts of width $\ell_{\alpha\beta\sigma} = \ell_{\gamma\delta} = 0.002a$.

The morphological diagram in Figure 6 is modified when thermal fluctuations are taken into account. In the absence of thermal fluctuations, we find metastable states in regimes IIb and III for a linophilic domain and in regimes IIb and I for a linophobic domain. In going from regimes II to III on a linophilic domain by *decreasing* ρ_V and from II to I on a linophobic domain by *increasing* ρ_V, the boundary minima at $\rho = \rho_V$ always remain metastable, which results in vertical instability lines located at $\Delta\lambda = 0$ in the morphological diagram in Figure 6a. In the presence of thermal fluctuations, however, barriers in the free energy profiles $f = f(\rho)$, which are induced by line tension contrasts and stabilize these states (see Figures 14 and 15 in Appendix B), can be overcome by thermal activation. If the barrier is smaller than T, we assume that these boundary states are mechanically stable but *unstable with respect to thermal activation*. Applying this criterion to all instability lines in the morphological diagram in
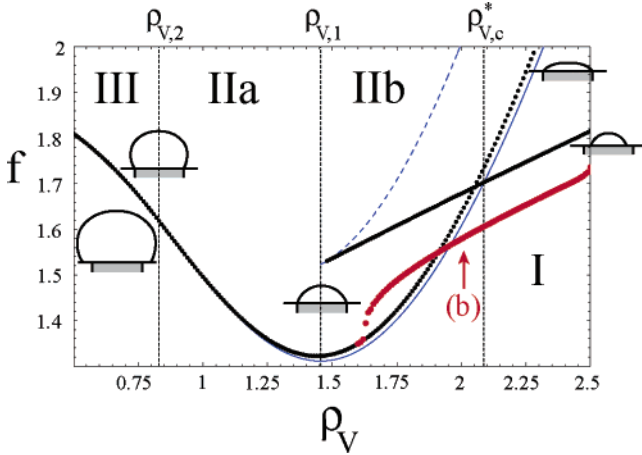
Figure 9. Plot of $\partial_\rho f(\rho)$ according to eq 39 for $w_\gamma = 0.5$, $w_\delta = -0.5$, $\lambda_\gamma = 0.1$, $\lambda_\delta = 0.2$, and $\ell_{\alpha\beta\sigma} = 0.05$ at the depinning transition $\rho_V = \rho_{V,c} \approx 0.536$. The discontinuity of $\partial_\rho f(\rho)$ at $\rho = \rho_V$ is due to the wettability contrast. Local free energy minima are $\rho_1 = \rho_V$, and $\rho_2 \approx 0.80$. The shading illustrates the Maxwell-like construction according to eq 40.

Figure 8. Linophobic domain. Free energy bifurcation diagram showing the global minima $f(\rho_{bo}) = f(\rho_{bo}(\rho_V))$ and the branches of metastable minima as a function of the dimensionless domain radius ρ_V (see eq 24), for $w_\gamma = 0.5$, $w_\delta = -0.5$, and $\lambda_\gamma = 0.2$, $\lambda_\delta = 0.1$. Blue lines: Analytic results for axisymmetric shapes and steplike line tension contrast. We find $\rho_{V,c}^* \simeq 2.087$, $\rho_{V,1} \simeq 1.528$, and $\rho_{V,2} \simeq 0.830$. The regimes I, IIa, IIb, and III according to eq 64 are indicated. The pinning and depinning transition between regimes IIa and III is continuous, the depinning from regimes II to regime I is discontinuous, the re-pinning from regime I to regimes II is continuous. The dashed blue line represents the branch of unstable free energy maxima. Black points: Results from numerical minimization restricted to axisymmetric shapes. Red points: Results from numerical minimization allowing for nonaxisymmetric shapes. The nonaxisymmetric shape in point b is shown in Figure 10b. Numerical results for continuous line tension and wettability contrasts of width $\ell_{\alpha\beta\sigma} = \ell_{\gamma\delta} = 0.002a$.

Figure 6a, we find the modified morphological diagrams, including thermal fluctuations, in Figure 6b, where the regimes containing metastable states are decreased in size. In regime III, for a linophilic domain and regime I for a linophobic domain, the size of the free energy barriers only depends on the line tension contrast and the domain size, but they are volume-independent, which leads again to vertical instability lines. These lines are shifted to $\Delta\lambda \sim \pm a^2/\ell_{mol}^2$ by thermal fluctuations. In the region between the shifted vertical lines around $\Delta\lambda = 0$, we can regard the depinning transitions as *quasi-continuous* (except for the case in which $\Delta\lambda = 0$, where it is strictly continuous); by thermal activation, the system can find its minimum *spontaneously* in this regime.

5.1.2. Nonaxisymmetric Shapes. As will be discussed in the last section, line tension contrasts can stabilize nonaxisymmetric shapes, both for $\Delta\lambda > 0$ and $\Delta\lambda < 0$, as shown in Figure 10a,b. Even in this case, there still exists a steplike free energy barrier that gives rise to morphological diagrams similar to those for axisymmetric shapes.

For the case of a *linophilic domain* $\Delta\lambda > 0$ (i.e., $\Lambda_\gamma < \Lambda_\delta$), the droplet tends to maximize its contact line length within the domain and, at the same time, cover the lyophilic domain. This leads to a "geometrically frustrated" situation for larger volumes, where the droplet wets the surrounding substrate δ, that is, for the states in regimes IIb and III (see Figure 7). They become unstable with respect to a displacement of the droplet relative to the circular domain such that the circular domain touches the droplet contact line, as indicated in Figure 10a. This breaks the axial symmetry of the problem. Such configurations become the global minimum in regime III and an energetically more favorable metastable branch in regime IIb. The free energy branch with broken axial symmetry is indicated in the free energy bifurcation diagram in Figure 7 (red curve). The broken axial symmetry also
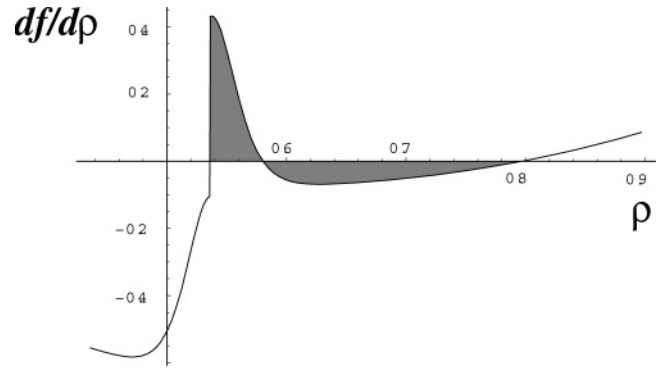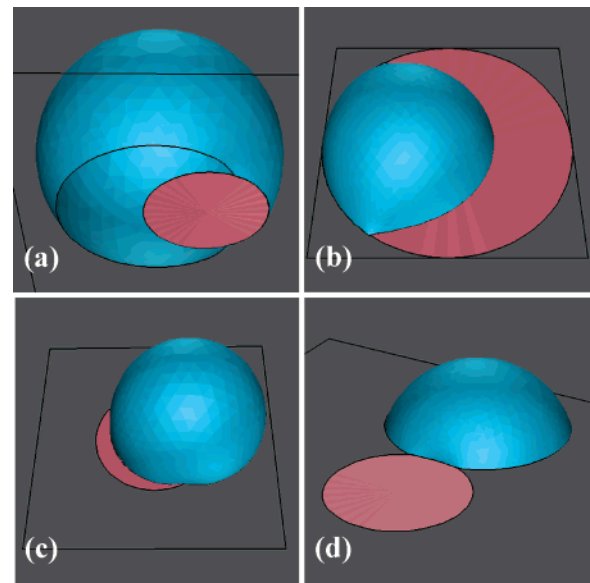

Figure 10. Nonaxisymmetric equilibrium droplet shapes stabilized by a line tension contrast on a planar substrate containing a circular domain (red): (a) for a lyophilic and linophilic domain ($w_\gamma = 0.5$, $w_\delta = -0.5$, $\lambda_\gamma = 0.1$, $\lambda_\delta = 0.2$) at $\rho_V = 0.5$. (b) for a lyophilic and linophobic domain ($w_\gamma = 0.5$, $w_\delta = -0.5$, $\lambda_\gamma = 0.2$, $\lambda_\delta = 0.1$) at $\rho_V = 2.0$. (c) for a linophilic domain *without* wettability contrast ($w_\gamma = w_\delta = 0$, $\lambda_\gamma = 0.1$, $\lambda_\delta = 0.2$) at $\rho_V = 0.9$. (d) for a *lyophobic* but linophilic domain ($w_\gamma = -0.5$, $w_\delta = 0.5$, $\lambda_\gamma = 0.1$, $\lambda_\delta = 0.2$) at $\rho_V = 1.1$.

changes the hysteresis behavior when the droplet approaches the depinning transition from large volumes or increasing ρ_V (i.e., when it re-pins). This re-pinning becomes *continuous* following the free energy branch with broken axisymmetry, that is, there is no "latent heat" released.

On the other hand, for a *linophobic domain* $\Delta\lambda < 0$ (i.e., $\Lambda_\gamma > \Lambda_\delta$), the droplet tends to maximize its contact line length outside the domain and, at the same time, cover the lyophilic domain. This leads to geometric frustration for smaller volumes, where the droplet is inside the γ-domain, that is, for the states in regimes I and IIb (see Figure 8). The droplet becomes unstable with respect to displacements to the boundary of the circular domain such that its contact line touches the embedding substrate outside of the domain, as shown in Figure 10b, thus breaking the axial symmetry. Such configurations become the global minimum in regime I and an energetically more favorable metastable branch in regime IIb. The free energy branch with

broken axial symmetry is indicated in the free energy bifurcation diagram in Figure 8 (red curve). Also, for this case, the broken axial symmetry modifies the hysteresis behavior when the droplet approaches the pinning transition from small volumes or decreasing ρ_V. This pinning becomes *continuous* following the free energy branch with broken axisymmetry, that is, there is no "latent heat" released.

5.2. Two-Valued Line Tension Contrast. In this section, we present analytical results for the two-valued steplike line tension contrast (eq 29) in addition to the wettability contrast with $w_\gamma > w_\delta$. Then the dimensionless free energy f of the spherical cap-shaped, axisymmetrically placed droplet is given by

$$f = f_\gamma = \frac{1}{2}\rho^2[1 + H^2(\rho)] - \frac{1}{2}w_\gamma\rho^2 + \lambda_\gamma\rho_V\rho \quad \text{for } \rho < \rho_V$$

$$f = f_\delta = \frac{1}{2}\rho^2[1 + H^2(\rho)] - \frac{1}{2}w_\delta\rho^2 + \lambda_\delta\rho_V\rho - \frac{1}{2}\rho_V^2(w_\gamma - w_\delta) \quad \text{for } \rho > \rho_V \quad (31)$$

where λ_γ and λ_δ stand for the values of λ, according to eq 25, in the lyophilic domain and in the lyophobic matrix, respectively.

We present a detailed analysis of the free energy $f = f(\rho)$ as given by eq 31 in Appendix B. The results of this analysis are presented in the following for the two cases of a linophilic domain ($\Lambda_\gamma < \Lambda_\delta$) and a linophobic domain ($\Lambda_\gamma < \Lambda_\delta$) separately. The results are summarized in the two bifurcation diagrams in Figures 7 and 8 (blue curves), where we plot the global and metastable minima of the free energy as a function of the volume control parameter ρ_V.

5.2.1. Line Tension Contrast $\Lambda_\gamma < \Lambda_\delta$ (Linophilic Domain). For a linophilic domain, there are now four regimes (I, IIa, IIb, and III) of wetting behavior, which are illustrated in the bifurcation diagram in Figure 7. The wetting behavior in regimes II and III is qualitatively changed compared to the case of a spatially homogeneous line tension due to steplike features in the free energy from the line tension contrast (see Figure 14, Appendix B).

For a linophilic domain, the behavior of the droplet within regime I for small volumes V_β or large ρ_V as well as the pinning transition between regimes I and II are exactly as those for a spatially homogeneous line tension $\lambda = \lambda_\gamma$, which has been discussed previously in section 4. Therefore, the contact angle of the droplet is the (weakly volume-dependent) contact angle θ_γ of the γ-domain in the presence of a line tension $\lambda = \lambda_\gamma$. Moreover, the pinning transition between regime I and II is *continuous*, as can also be seen in the smooth behavior of the global minimum of the free energy as a function of ρ_V in the bifurcation diagram in Figure 7. Upon increasing the volume or decreasing ρ_V, the droplet gets pinned to the $\gamma\delta$ domain boundary at a boundary volume V_1 corresponding to an upper boundary value $\rho_{V,1}$, which is calculated in Appendix B (see eq 59). The corresponding boundary contact angle is given by

$$\cos\theta_1 = w_\gamma - \lambda_\gamma \quad (32)$$

(see eq 58).

Within regime II, where the contact line is pinned at the domain boundary, the behavior becomes qualitatively different from that for a homogeneous line tension because of the discontinuity $\Delta f = \rho_V^2(\lambda_\delta - \lambda_\gamma)$ (see eq 57) in the free energy profiles $f = f(\rho)$. This steplike feature increases the stability of the boundary minimum corresponding to the pinned droplet with $r = a$ or $\rho = \rho_V$, which leads to the existence of a new regime IIb, where

the boundary minimum remains stable, although there already exists a metastable minimum corresponding to a droplet wetting the δ-substrate and covering the γ-domain. This metastable minimum appears above the boundary volume V_2, that is, for values $\rho_V < \rho_{V,2}$, where $\rho_{V,2}$ is given by eq 61, as calculated in Appendix B. The corresponding boundary contact angle is given by

$$\cos\theta_2 = w_\delta - \lambda_\delta \quad (33)$$

(see eq 60). The lower boundary value $\rho_{V,2}$ is identical to the boundary value obtained for the pinning of a droplet wetting the δ-domain and completely covering the γ-domain and with a homogeneous line tension $\lambda = \lambda_\delta$. Within the regime $\rho_{V,2} \le \rho_V \le \rho_{V,1}$, the droplet is in regime IIa, and the boundary minimum at $\rho_{bo} = \rho_V$ is the *only* free energy minimum (see Figure 7).

Upon further increasing the volume, the droplet enters regime IIb for $\rho_{V,c} < \rho_V < \rho_{V,2}$, where the boundary minimum is still the global minimum, but the metastable minimum appears corresponding to a droplet wetting the δ-matrix. As can be seen in Figure 7, the two minima exchange stability at a *critical value* $\rho_{V,c}$ corresponding to a critical volume V_c and a contact angle θ_c, which can only be determined numerically. At this critical volume, a *discontinuous depinning transition* takes place into regime III with a jump, $\Delta\rho_{bo} > 0$, in the equilibrium contact radius. The size of this jump is estimated in Appendix B.3 in eq 69. This jump also leads to a corresponding discontinuity, $\Delta\theta \equiv \theta_\delta - \theta_c < 0$, in the equilibrium contact angle. θ_δ is the (weakly volume-dependent) contact angle of a droplet wetting the δ-substrate in the presence of a line tension, $\lambda = \lambda_\delta$. For the contact angle discontinuity we find

$$\Delta\theta \approx -2^{1/6}\rho_{V,c}(\lambda_\delta - \lambda_\gamma)^{1/2}(1 - w_\delta)^{2/3}(2 + w_\delta)^{5/6} \quad (34)$$

in eq 70 in Appendix B. Thus, the discontinuity in the contact angle at the discontinuous depinning transition of the contact line depends on (i) the critical droplet volume, (ii) the line tension contrast, and (iii) the wettability or contact angle of the δ-substrate. In the entire regime II (i.e., for $\rho_{V,c} < \rho_V \le \rho_{V,1}$), the equilibrium contact line is pinned, and the contact angle varies with the volume in the range $\theta_1 \le \theta < \theta_c$, according to the relation given in eq 28.

In regime III, for large volumes or small $\rho_V < \rho_{V,c}$, the droplet wets the δ-substrate in its equilibrium shape. Note, however, that, in the absence of thermal fluctuations, the bound state remains metastable within the entire regime III. This leads to the pronounced hysteresis displayed in the bifurcation diagram in Figure 7. The contact angle in this metastable state can increase dramatically by following the relation in eq 28 for all $\rho_V \le \rho_{V,2}$. Because the boundary state does not get mechanically unstable for increasing volume, the actual depinning transition has to be enabled by thermal fluctuations or some other external perturbation, which will be discussed below. It also means that the corresponding spinodal or instability line of the transition cannot be accessed by decreasing ρ_V. This results in a vertical second instability line, $\Delta\lambda = 0$, in the morphological diagram in Figure 6.

Upon approaching the pinning transition from the large volume regime III by increasing ρ_V (i.e., upon re-pinning), the local minimum corresponding to a droplet wetting the δ-substrate remains metastable for $\rho_{V,c} < \rho_V < \rho_{V,2}$. Therefore, the other spinodal or instability line is given by $\rho_V = \rho_{V,2}$. It should also be noted that, for sharp line tension contrasts, there is practically *no* discontinuity in the equilibrium radius ρ or in the contact angle upon re-pinning at $\rho_V = \rho_{V,2}$. Thus, the re-pinning transition

will appear continuous, although there is a discontinuity in the free energy, that is, there is a "latent heat" released.

5.2.2. Line Tension Contrast $\Lambda_\gamma > \Lambda_\delta$ (Linophobic Domain). We can perform an analogous analysis for a linophobic domain, which also exhibits four regimes (I, IIa, IIb, and III) of wetting behavior, which are illustrated in the bifurcation diagram in Figure 8 (blue curves). It turns out that the depinning behavior for the linophilic domain for *increasing* volume, which we treated in the previous section, is qualitatively similar to the depinning behavior for the linophobic domain for *decreasing* volume. In both cases, the contact line depins discontinuously from the boundary of the circular domain upon entering into the region with the less favorable line tension. These similarities are also obvious from comparing the basic structure of the bifurcation diagrams in Figures 7 and 8. Accordingly, for the linophobic domain, the wetting behavior in regimes I and II is qualitatively changed compared to that in the case of a spatially homogeneous line tension due to steplike features in the free energy (see Figure 15, Appendix B).

The behavior of the droplet within regime III for large volumes V_β or small ρ_V as well as the pinning transition between regimes III and II are exactly the same as those for a spatially homogeneous line tension, $\lambda = \lambda_\delta$, which has been discussed previously in section 4. The contact angle of the droplet is the (weakly volume-dependent) contact angle θ_δ wetting the δ-substrate in the presence of a line tension $\lambda = \lambda_\delta$. The pinning transition between regimes III and II is *continuous*, as can also be seen in the smooth behavior of the global minimum of the free energy as a function of ρ_V in the bifurcation diagram in Figure 8. Upon decreasing the volume or increasing ρ_V, the droplet gets pinned to the $\gamma\delta$ domain boundary at a boundary volume V_2 corresponding to a lower boundary value $\rho_{V,2}$, which is given by eq 61 as calculated in Appendix B. The corresponding boundary contact angle is given by

$$\cos \theta_2 = w_\delta - \lambda_\delta \qquad (35)$$

Within regime II, where the contact line is pinned at the domain boundary, the behavior becomes qualitatively different from that for a homogeneous line tension because of the discontinuity in the free energy profiles. This steplike feature increases the stability of the boundary minimum corresponding to the pinned droplet with $r = a$ or $\rho = \rho_V$, which leads to the existence of a new regime IIb, where the boundary minimum remains stable, although there already exists a metastable minimum corresponding to a droplet sitting within the γ-domain. This metastable minimum appears below the boundary volume V_1 (i.e., for values $\rho_V > \rho_{V,1}$), where $\rho_{V,1}$ is given by eq 59. The corresponding boundary contact angle is given by

$$\cos \theta_1 = w_\gamma - \lambda_\gamma \qquad (36)$$

The upper boundary value $\rho_{V,1}$ is identical to the boundary value obtained for the pinning of a droplet sitting within the γ-domain and with a homogeneous line tension, $\lambda = \lambda_\gamma$. Within the regime $\rho_{V,2} \leq \rho_V \leq \rho_{V,1}$, the droplet is in regime IIa, and the boundary minimum at $\rho_{bo} = \rho_V$ is the *only* free energy minimum (see Figure 8).

Upon further decreasing the volume, the droplet enters regime IIb for $\rho_{V,1} < \rho_V < \rho_{V,c}^*$, where the boundary minimum is still the global minimum, but the metastable minimum appears, corresponding to a droplet sitting within the γ-domain. As can be seen in Figure 7, the two minima exchange stability at a *critical value* $\rho_{V,c}^*$ corresponding to a critical volume V_c^* and a critical contact angle θ_c^*. At this critical volume, a *discontinuous*

depinning transition into regime I takes place with a jump, $\Delta\rho_{bo}^* < 0$, in the equilibrium contact radius. The size of this jump is estimated in Appendix B.3 in eq 71. This jump also leads to a corresponding discontinuity, $\Delta\theta^* \equiv \theta_\gamma - \theta_c^* > 0$, in the equilibrium contact angle. θ_γ is the (weakly volume-dependent) contact angle of a droplet in the γ-domain in the presence of a line tension, $\lambda = \lambda_\gamma$. For the contact angle discontinuity, we find

$$\Delta\theta^* \approx 2^{1/6}\rho_{V,c}^*(\lambda_\delta - \lambda_\gamma)^{1/2}(1 - w_\gamma)^{2/3}(2 + w_\gamma)^{5/6} \quad (37)$$

in eq 71 in Appendix B. In the entire regime II (i.e., for $\rho_{V,2} < \rho_V \leq \rho_{V,c}^*$), the equilibrium contact line is pinned, and the contact angle varies with the volume in the range $\theta_c^* \leq \theta < \theta_2$ according to the relation in eq 28.

In regime I, for small volumes or large $\rho_V > \rho_{V,c}^*$, the droplet is on the γ-domain in its equilibrium shape. Note, however, that, in the absence of thermal fluctuations, the bound state remains metastable within the entire regime I. This leads to the pronounced hysteresis displayed in the bifurcation diagram in Figure 8. The contact angle in this metastable state can decrease dramatically by following the relation in eq 28 for all $\rho_V \geq \rho_{V,1}$. Because the boundary state does not get mechanically unstable for decreasing volume, the actual depinning transition has to be enabled by thermal fluctuations or some other external perturbation, which will be discussed below. It also means that the corresponding spinodal or instability line of the transition cannot be accessed by increasing ρ_V. This results in a vertical second instability line, $\Delta\lambda = 0$, in the morphological diagram in Figure 6.

Upon approaching the pinning transition from the small volume regime I by decreasing ρ_V (i.e., upon re-pinning), the local minimum corresponding to a droplet within the γ-domain remains metastable for $\rho_{V,1} < \rho_V < \rho_{V,c}^*$. Therefore, the other spinodal or instability line is given by $\rho_V = \rho_{V,1}$. It should also be noted that, for sharp line tension contrasts, there is practically *no* discontinuity in the equilibrium radius ρ or in the contact angle upon re-pinning at $\rho_V = \rho_{V,1}$. Thus, the re-pinning transition will appear continuous, although there is a discontinuity in the free energy, that is, there is a "latent heat" released.

5.3. Continuous Line Tension Contrast and Maxwell-like Construction. So far we have considered the situation of a sharp line tension contrast (eq 29). Then the boundary minimum at $\rho = \rho_V$ remains a metastable minimum throughout the entire regimes I or III for linophobic and linophilic domains, respectively, and the pinned contact line never becomes mechanically unstable with respect to depinning. In this situation, contact line depinning has to happen by additional external forces acting on the droplet, for example, thermal noise.

In a more realistic model, the line tension contrast is *continuous*, that is, the line tension step is smeared over a characteristic width, which is given by the width of the contact line $\ell_{\alpha\beta\sigma}$ (see eq 30), which can be written as

$$\lambda(\rho) = \frac{\lambda_\delta - \lambda_\gamma}{2} \tanh\left(\frac{\rho/\rho_V - 1}{\bar{\ell}_{\alpha\beta\sigma}}\right) + \frac{\lambda_\delta + \lambda_\gamma}{2} \qquad (38)$$

using dimensionless quantities with $\ell_{\alpha\beta\sigma} \equiv \bar{\ell}_{\alpha\beta\sigma}/a$. Then the dimensionless free energy of the droplet f is given by

$$f = \frac{1}{2}\rho^2[1 + H^2(\rho)] - \frac{1}{2}w(\rho)\rho^2 + \lambda(\rho)\rho_V\rho + \Theta(\rho - \rho_V)\frac{1}{2}\rho_V^2$$
$$(w_\gamma - w_\delta) \quad (39)$$

where $w(\rho) = w_\gamma + \Theta(\rho - \rho_V)(w_\delta - w_\gamma)$. For a continuous line

tension contrast, the free energy (eq 39) has no discontinuity across $\rho = \rho_V$.

We find that the results for a continuous line tension contrast are qualitatively the same as those for a steplike two-valued line tension contrast. In particular, we find the same three regimes following the global minimum $\rho_{bo} > 0$ of the free energy (eq 31) as a function of the dimensionless surface domain radius ρ_V. The notable difference is that the global minimum in regime II is not necessarily the boundary minimum at $\rho = \rho_V$, but it can also become a local minimum. Then two local minima exchange their stability at the discontinuous depinning transition of the contact line at the critical value of ρ_V.

Because the free energy (eq 39) has no discontinuities, we can obtain the critical values $\rho_{V,c}$ or $\rho_{V,c}^*$ for the discontinuous depinning transitions from a Maxwell-like construction, which we illustrate for the linophilic case, $\Lambda_\gamma < \Lambda_\delta$. At the transition at $\rho_V = \rho_{V,c}$, the locations of the two local minima are $\rho_1 < \rho_V$, where ρ_1 is within the γ-domain and determined by $\partial_\rho f_\gamma(\rho_1) = 0$ or $\rho_1 = \rho_V$, on one hand, and $\rho_2 > \rho_V$ on the δ-substrate, with $\partial_\rho f_\delta(\rho_2) = 0$, on the other hand. The corresponding free energies are equal at the transition, that is,

$$0 = f_\gamma(\rho_1) - f_\delta(\rho_2) = \int_{\rho_1}^{\rho_2} d\rho\, \partial_\rho f$$

$$= \int_{\rho_1}^{\rho_2} d\rho\rho \left[\cos\theta(\rho) - w(\rho) + \frac{\rho_V \lambda(\rho)}{\rho} + \rho_V \partial_\rho \lambda \right] \quad (40)$$

which leads to a Maxwell-like construction, in which we locate the critical value $\rho_{V,c}$ by requiring that the curve $\partial_\rho f(\rho)$ intersect three times with the line $\partial_\rho f(\rho) = 0$ (i.e., at ρ_1, ρ_2, and an intermediate point ρ_i, corresponding to an unstable free energy maximum), and that the areas $|\int_{\rho_1}^{\rho_i} \partial_\rho f(\rho)|$ and $|\int_{\rho_i}^{\rho_2} \partial_\rho f(\rho)|$ of the curve above and below zero are equal (see Figure 9).

For ρ_V only slightly below $\rho_{V,c}$, the local minimum at $\rho = \rho_1$ remains metastable. Whereas, for a two-valued line tension contrast, this minimum was always a boundary minimum ($\rho_1 = \rho_V$) and remained metastable for *all* $\rho_V < \rho_{V,c}$, the minimum at ρ_1 can become mechanically unstable at a lower value, $\rho_V = \rho_{V,s} < \rho_{V,c}$, for a continuous line tension contrast. The value $\rho_{V,s}$ is determined by the two conditions $\partial_\rho f(\rho_1) = 0$, which is the contact line equation for the γ-domain, and $\partial_\rho^2 f(\rho_1) = 0$. These conditions can only be fulfilled for a sufficiently smooth line tension contrast, that is, for a sufficiently large $\ell_{\alpha\beta\sigma}$. The maximal gradient in line tension is attained for $\rho \sim \rho_V$ and is approximately given by $\partial_\rho \lambda(\rho_V) \sim (\Lambda_\delta - \Lambda_\gamma)/\Sigma_{\alpha\beta}\ell_{\alpha\beta\sigma}$. A sufficient condition for the local minimum at $\rho = \rho_1$ to become unstable is that no boundary minimum $\rho_1 = \rho_V$ exists (i.e., $\partial_\rho f(\rho_V) < 0$ with $w(\rho_V) = w_\delta$), which gives

$$\frac{\Lambda_\delta - \Lambda_\gamma}{2\Sigma_{\alpha\beta}\ell_{\alpha\beta\sigma}} = \frac{\lambda_\delta - \lambda_\gamma}{2\bar{\ell}_{\alpha\beta\sigma}} < 1 + w_\delta - \lambda_\delta \quad (41)$$

For large line tension contrasts or a small contrast width, $\bar{\ell}_{\alpha\beta\sigma}$, this condition is violated and, thus, the boundary minimum at $\rho = \rho_V$ *never* becomes mechanically unstable like that for a steplike line tension contrast. One can also show that, in this case, there is a small range of radii, $\rho_V < \rho < \rho_V + \bar{\ell}_{\alpha\beta\sigma}$, where there *never* exists a solution to the contact line equation, that is, a "forbidden" range of radii where it is not possible to find an axisymmetric solution to the contact line equation. This paradox can only be resolved by including nonaxisymmetric shapes into the analysis, as will be done in section 5.5.

5.4. Thermal Fluctuations. The morphological diagram in Figure 6a is valid for a sharp line tension contrast (eq 29) or a

continuous contrast (eq 38), provided that the contrast width $\bar{\ell}_{\alpha\beta\sigma}$ is small enough, as discussed above. In the absence of thermal fluctuations, we find metastable states in regimes IIb and III for a linophilic domain and in regimes IIb and I for a linophobic domain. Moreover, we found that the metastable states in regime III (for the *linophilic* case) and in regime I (for the *linophobic* case) *never* become mechanically unstable in the absence of external perturbations. However, as discussed in section 5.1, in the presence of thermal fluctuations some of these states can become unstable with respect to *thermal activation*. In the following, we derive the condition for an instability with respect to thermal activation and the resulting changes in the morphological diagram in Figure 6.

Thermal activation over an energy barrier ΔF involves thermally activated shape changes of the droplet at a constant liquid volume V_β. Thermally activated nucleation processes, which involve the deposition of liquid and thus volume growth, have been studied in the literature in the framework of classical nucleation theory,[31] for example, nucleation on homogeneous substrates[32] or circular domains.[33,34] We assume that similar concepts can describe thermally activated shape changes, which then proceed with a rate J proportional to the Arrhenius factor,

$$J = J_0 \exp(-\Delta F/T) \quad (42)$$

where the prefactor J_0 depends on the details of the kinetic mechanisms involved in the shape changes. Therefore, a reasonable criterion for the instability with respect to thermal activation is to assume that barriers $\Delta F \lesssim T$ can be overcome by thermal activation on the experimental time scale. Using dimensionless units (eq 12), this leads to a condition

$$\Delta f = T/2\pi\Sigma_{\alpha\beta}L_\beta^2 \sim \ell_{mol}^2/2\pi L_\beta^2 = \rho_V^2 \ell_{mol}^2/2\pi a^2 \quad (43)$$

which determines the instability lines in the presence of thermal fluctuations and where we used the approximation $\Sigma_{\alpha\beta} \sim (T/\ell_{mol}^3)/\alpha\beta \sim T/\ell_{mol}^2$, as discussed in section 2.2. Using this criterion (eq 43), we obtain the modified instability lines in the morphological diagram in Figure 6b in regimes IIb and III for a linophilic domain and regimes IIb and I for a linophobic domain.

First we consider the metastable states within regime III for a linophilic domain or regime I for a linophobic domain, which do not become mechanically unstable in the absence of thermal fluctuations. The line tension contrast gives rise to steplike discontinuities in the free energy (see Figures 14 and 15, Appendix B). Assuming axisymmetric shapes throughout the thermal activation process, the free energy barrier that these metastable states have to overcome is given by

$$\Delta f = |f_\delta(\rho_V) - f_\gamma(\rho_V)| = \rho_V^2 |\lambda_\delta - \lambda_\gamma| \quad (44)$$

(see also eq 57), or $\Delta F = 2\pi a |\Lambda_\delta - \Lambda_\gamma|$ in original units, which shows that this free energy barrier is volume-independent. Using eq 44, the condition (eq 43) for the instability lines becomes

$$|\Delta\lambda| = \ell_{mol}^2/2\pi a^2 \quad (45)$$

which is independent of volume or ρ_V and, thus, again gives two *vertical* instability lines in the morphological diagram in Figure 6b. Compared to the morphological diagram in Figure

(31) Frenkel, J. *Kinetic Theory of Liquids*; Dover: New York, 1955.
(32) McDonald, J. E. *Am. J. Phys.* **1963**, *31*, 31.
(33) Smorodin, V. E. *Langmuir* **1994**, *10*, 2250.
(34) Valencia, A.; Lipowsky, R. *Langmuir* **2000**, *20*, 1986.

6a, in the absence of thermal fluctuations, both of the vertical instability lines are shifted. In the region between the shifted vertical lines around $\Delta\lambda = 0$, we can regard the depinning transitions as *quasi-continuous* (except for the case in which $\Delta\lambda = 0$, where it is strictly continuous); by thermal activation, the system can find its minimum *spontaneously* in this regime.

Similarly, we can apply the criterion in eq 43 to the other instability lines, $\rho_V = \rho_{V,2}$ for a linophilic domain and $\rho_V = \rho_{V,1}$ for a linophobic domain. In the morphological diagram in Figure 6b, the resulting shifted instability lines have been calculated numerically for $a = 10\ell_{mol}$ using the criterion in eq 43. For both $\Delta\lambda > 0$ and $\Delta\lambda < 0$, the modified instability lines meet at a single point for a small line tension contrast, where minima exchange stability and the energy barrier separating them is of height T.

From the criterion given in eq 43, we recognize that thermal fluctuation effects are essentially governed by the ratio ℓ_{mol}/a. With ℓ_{mol} being on the order of 1 nm, effects from thermal fluctuations should be small, even for the smallest realistic domain sizes, which are on the order of 10 nm. This is also clearly seen in the morphological diagram in Figure 6b, where the shift of the instability lines is rather small for $a = 10\ell_{mol}$. It should also be noted that the energy barriers between metastable states can be further reduced by breaking the axial symmetry, as we will see in the next section.

5.5. Numerical Minimization and Nonaxisymmetric Shapes. Although the problem of a droplet on a single circular lyophilic domain has axial symmetry, equilibrium droplet shapes can break this symmetry in the presence of a *line tension contrast*. In Figure 10, we give an overview of possible nonaxisymmetric droplet shapes, which are stabilized by a line tension contrast. For a smaller linophilic domain, large droplets that wet the lyophobic substrate are unstable with respect to displacements such that they touch the domain boundary (Figure 10a). For a linophobic domain, small droplets on the lyophilic domain are unstable with respect to displacements such that they touch the domain boundary (Figure 10b). Also, in the absence of a wettability contrast, droplets on a linophilic domain are unstable with respect to displacements in order to maximize the length of their contact line on the domain (Figure 10c). Obviously, for a lyophobic domain in a lyophilic substrate, droplets preferentially nucleate and attach outside of the domain on the lyophilic substrate, thus breaking the axial symmetry also in the absence of a line tension contrast. In this case, a linophilic domain can stabilize states where the droplet partially covers the lyophobic domain (Figure 10d). In this paper, we want to focus on lyophilic domains embedded in a lyophobic substrate, that is, cases a and b of Figure 10.

5.5.1. Numerical Minimization. For nonaxisymmetric droplet shapes, analytical calculations are no longer feasible, and we resort to numerical minimization of the droplet free energy using the dynamical triangulation algorithms of the freely available SURFACE EVOLVER 2.14.[35] The numerical minimization of the free energy functional (eq 1) is performed at a fixed volume V_β or a fixed ρ_V. Using the additional constraint for the center of mass of the contact line to lie in the center of the circular domain, the minimum stays within the subspace of axisymmetric shapes. Lifting this constraint, we can also access nonaxisymmetric shapes. Using these techniques, we first confirmed our analytical result for the global and metastable minima of the free energy in the subspace of axisymmetric shapes for steplike wettability and line-tension contrasts. Numerically, we approximate steplike contrasts by continuous contrasts of the form given in eq 30 and make the line tension contrast width $\ell_{\alpha\beta\sigma}$ and
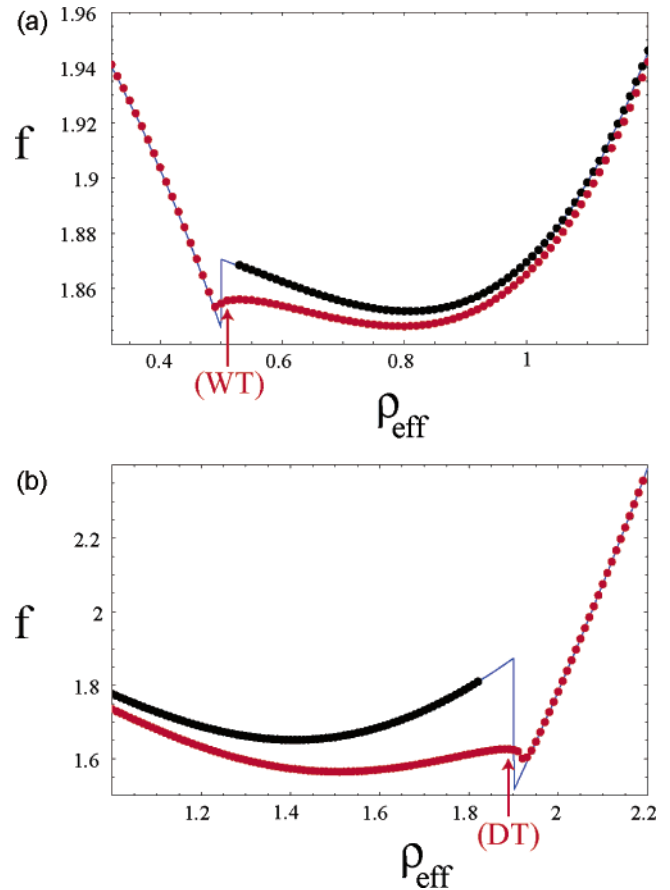
(35) Brakke, K. *Exp. Math.* **1992**, *1*, 141.

Figure 11. (a) Linophilic domain. Free energy $f = f(\rho_{eff})$ as a function of the effective dimensionless droplet radius ρ_{eff} (see eq 46), for $\rho_V = 0.5$ and $w_\gamma = 0.5$, $w_\delta = -0.5$, $\lambda_\gamma = 0.1$, and $\lambda_\delta = 0.2$. (b) Linophobic domain. Free energy $f = f(\rho_{eff})$ for $\rho_V = 1.9$ and $w_\gamma = 0.5$, $w_\delta = -0.5$, $\lambda_\gamma = 0.2$, and $\lambda_\delta = 0.1$. Blue: Analytic results for axisymmetric shapes and steplike line tension contrast. Black: Results from numerical minimization restricted to symmetric shapes. Red: Results from numerical minimization allowing for nonaxisymmetric shapes. Numerical results for continuous line tension and wettability contrasts of width $\ell_{\alpha\beta\sigma} = \ell_{\gamma\delta} = 0.01a$. The nonaxisymmetric constrained equilibrium shapes of droplets representing the "transition states" of a "wet tongue" (WT) or a "dry tongue" (DT) are shown in Figure 12.

the wettability contrast width $\ell_{\gamma\delta}$ as small as the numerical stability of the algorithm allows.

To confirm our analytical results on the free energy bifurcation diagrams for the pinning and depinning transitions in the presence of line tension contrasts, we first perform a numerical minimization of the free energy for axisymmetric shapes. As can be seen in Figures 7 and 8, the agreement is good. Small differences in Figure 8 are due to the finite width of the continuous contrasts used for numerical minimization.

5.5.2. Nonaxisymmetric Shapes Stabilized by Line Tension Contrasts. As we already discussed in 5.1, nonaxisymmetric droplet shapes can be stabilized by a line tension contrast and provide more favorable metastable and global minima in regimes IIb and III for the linophilic case (see Figure 7) and in regimes IIb and I for the linophobic case (see Figure 8). These shapes assume the form indicated in Figure 10a for a linophilic domain (see also arrow in Figure 7) and in Figure 10b for a linophobic domain (see arrow in Figure 8).

Furthermore, for axisymmetric shapes, we found a window of radii $\rho_V < \rho < \rho_V + \ell_{\alpha\beta\sigma}$ for the linophilic case, where it is not possible to find an axisymmetric solution to the Young equation for large line tension gradients. The contact line of
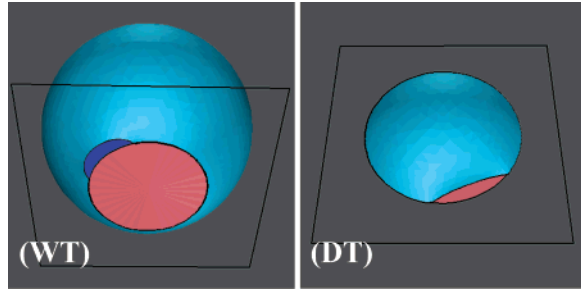
Figure 12. Constrained equilibrium shapes of droplets representing the "transition states" at the top of the energy barriers in Figure 11. (WT) Droplet configuration with a "wet tongue" (dark blue area) for $\rho_V = 0.5$ and $w_\gamma = 0.5$, $w_\delta = -0.5$, $\lambda_\gamma = 0.1$, and $\lambda_\delta = 0.2$ at $\rho_{eff} = 0.51$. (DT) Droplet configuration with a "dry tongue" for $\rho_V = 1.9$ and $w_\gamma = 0.5$, $w_\delta = -0.5$, $\lambda_\gamma = 0.2$, and $\lambda_\delta = 0.1$ at $\rho_{eff} = 1.88$.

nonaxisymmetric solutions such as the equilibrium shape shown in Figure 10a, however, clearly crosses this ring-shaped "forbidden" region. These shapes can fulfill the Young equation (eq 3) because the contact line crosses this region with an angle with respect to the domain boundary, which is sufficiently close to $\pi/2$ such that the scalar product $\hat{\mathbf{m}} \cdot \nabla \Lambda / \Sigma_{\alpha\beta}$ in the last term of the Young equation becomes small. Thus, a solution fulfilling $-1 < \cos \theta < 1$ can be found.

5.5.3. Resolving the Bifurcations. By applying a constraint on the adhered area $A_{\beta\sigma}$ of the droplet, we can numerically resolve the constrained free energy landscape as a function of an *effective* dimensionless radius

$$\rho_{eff} \equiv (A_{\beta\sigma}/\pi L_\beta^2)^{1/2} \qquad (46)$$

at fixed ρ_V. For axisymmetric droplet shapes the effective radius coincides with the radius ρ (i.e., $\rho_{eff} = \rho$), and we can compare numerical results with the corresponding free energy profiles for $f = f(\rho)$ as given by eq 31 and displayed in Figures 14 and 15 (Appendix B).

In Figure 11a, we show a detailed comparison of the constrained free energy profiles for a linophilic domain and a droplet volume close to the transition, that is, at the boundary between regimes IIb and III. If we constrain the numerical minimization to axially symmetric shapes (black points), we get good agreement with the analytical results (blue line). Close to the free energy maximum, the axisymmetric shape is hard to stabilize in the numerical minimization such that the data points are missing in this region. For axisymmetric shapes, the energy barrier separating the competing minima is given by the step (eq 44) in free energy. However, this barrier is drastically *reduced* if we allow for shapes breaking the axial symmetry in the numerical minimization (red points in Figure 11). Typical nonaxisymmetric shapes for ρ_{eff} slightly larger than ρ_V (i.e., for small positive $\Delta\rho_{eff} \equiv \rho_{eff} - \rho_V$) exhibit a single "tongue"-like protrusion (see Figure 12), which is formed from the excess adhered area $\Delta A = \pi L_\beta^2 (\rho_{eff}^2 - \rho_V^2)$ that cannot fit on the lyophilic domain and extends into the lyophobic substrate. The excess adhered area assumes a compact shape similar to a half-circle in order to minimize the length of the excess contact line ΔL, which becomes subject to the higher line tension λ_δ of the surrounding substrate. Therefore, we expect $\Delta L \sim (2\pi\Delta A)^{1/2}$. Formation of the tongue is favored by the free energy gain from decreasing the area of the $\alpha\beta$ interface. This free energy gain is linear in $\Delta\rho_{eff}$ and proportional to $\Sigma_{\alpha\beta}$. Then the total change in dimensionless free energy, Δf, due to the formation of the tongue can be estimated as

$$\Delta f(\Delta\rho_{eff}) \sim -c\rho_V\Delta\rho_{eff} + (w_\delta - w_\gamma)\rho_V\Delta\rho_{eff} + (\lambda_\delta - \lambda_\gamma)\rho_V^{3/2}\Delta\rho_{eff}^{1/2} \qquad (47)$$

where c is a numerical constant of order unity. For small $\Delta\rho_{eff}$, the term from the line tension cost ($\propto \Delta\rho_{eff}^{1/2}$) dominates and gives rise to an energy barrier

$$\Delta f \sim \frac{\rho_V^2(\lambda_\delta - \lambda_\gamma)^2}{c} \qquad (48)$$

which is, by a factor of $\lambda_\delta - \lambda_\gamma \ll 1$, smaller than the result (eq 44) for axisymmetric shapes. The droplet shape in the "transition state" (i.e., the constrained equilibrium configuration at the top of the barrier) is shown in Figure 12(WT). Although the barrier is reduced, it is also still existing if we include nonaxisymmetric shapes into the analysis. Therefore, the pinned state of the droplet at the boundary minimum, $\rho_{bo} = \rho_V$, *never* becomes mechanically unstable upon approaching the depinning transition from small volumes (i.e., decreasing ρ_V), even if we allow for nonaxisymmetric shapes (for the zero temperature case).

In Figure 11b, we show the analogous comparison of the constrained free energy profiles for a linophobic domain and a droplet volume close to the transition, that is, at the boundary between regimes IIb and I. For this type of contrast and typical nonaxisymmetric shapes with ρ_{eff} slightly smaller than ρ_V, the droplet pulls back from the circular domain where the line tension is high, leaving a "dry tongue" behind (see Figure 12(DT)). We can use arguments analogous to those in the previous section in order to estimate the barrier height that is associated with the formation of such a "dry tongue", which leads to the same result (eq 48). Also, in this case, a barrier persists if the axial symmetry can be broken by the transition states.

From Figure 11, we also recognize that, for both types of line tension contrasts, the discontinuity ($\Delta\rho_{bo}$ or $\Delta\rho_{bo}^*$) of the dimensionless radius at the depinning transitions (see eqs 69 and 71 in Appendix B.3) is not significantly modified if nonaxisymmetric shapes are taken into account.

6. Summary and Discussion

We studied line tension effects for a single droplet wetting a lyophilic circular domain γ embedded in a lyophobic substrate δ in the presence of a line tension contrast. By analyzing the interfacial and line free energies of the droplet, we found that a line tension contrast gives rise to *discontinuous* depinning transitions of the contact line from the domain boundary and thus leads to pronounced *hysteric* behavior. For a line tension contrast $\Lambda_\gamma < \Lambda_\delta$ (linophilic domain), the depinning from the domain boundary upon increasing the droplet volume becomes discontinuous, whereas, for a line tension contrast $\Lambda_\gamma > \Lambda_\delta$ (linophobic domain), the depinning upon decreasing the droplet volume becomes discontinuous. In both cases, we obtain the full bifurcation diagram for the free energy analytically and numerically for axisymmetric shapes.

Numerically, we also addressed instabilities with respect to axial symmetry breaking. In the presence of a line tension contrast, we find instabilities in the global and metastable equilibrium shapes in the regimes where the droplet has spread onto the part of the surface with the higher line tension, that is, for a linophilic domain if the droplet wets the surrounding linophobic substrate at large volume, or for a linophobic domain if the droplet resides entirely within this domain for small volumes (see Figure 10). The broken axisymmetry leads to a lowering of the corresponding free energy branches in the bifurcation diagram, which makes re-pinning transitions *continuous*. Axial symmetry breaking also
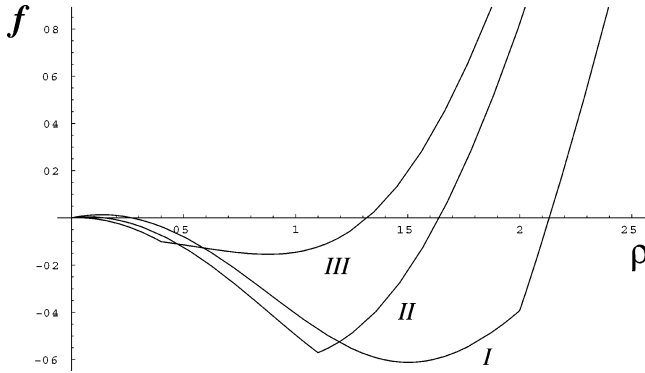
Figure 13. Plots of $f(\rho) - f(0)$ according to eq 26 for $w_\gamma = 0.5$, $w_\delta = -0.5$, and $\lambda = 0.1$. Plots from right to left are for $\rho_V = 2.0$, 1.1, and 0.4, i.e., for increasing volume corresponding to the three regimes in eq 56. In all three regimes, $f = f_\gamma$ for $\rho < \rho_V$ and $f = f_\delta$ for $\rho > \rho_V$, according to eq 26.

strongly reduces the barrier between metastable and global minima close to the transition.

These results suggest several experimental avenues to detect and eventually quantify line tension contrasts. The discontinuous nature of depinning transitions in the presence of a line tension contrast leads to a hysteretic behavior of the contact line, which should be observable in experiments. The hysteretic behavior as displayed in the bifurcation diagrams in Figures 7 and 8 for a linophilic and linophobic domain, respectively, can then be used to (i) determine the sign of the line tension contrast, that is, to detect whether the domain is linophilic or linophobic, and (ii) to quantify the size of the line tension contrast (see eqs 34 and 37). Moreover, line tension contrasts always lead to instabilities with respect to axial symmetry breaking in regimes where the droplet is spreading onto the part of the surface with the higher line tension. Observation of droplet shapes as shown in Figure 10 are thus an indicator for the presence of a line tension contrast. The shapes are also indicative of the sign of the line tension contrast: A linophilic domain will exhibit nonaxisymmetric shapes at large volumes where the droplet spreads on the surrounding linophobic substrate, whereas a linophobic domain exhibits such shapes at small volumes where the droplet resides entirely within this domain.

Appendix A. Free Energy Analysis for Circular Lyophilic Domains and Spatially Homogeneous Line Tension

In this appendix, we present the detailed analysis of the free energy $f = f(\rho)$ as given by eq 26 for an axisymmetrical spherical cap-shaped droplet on a circular lyophilic domain. Although the function $f(\rho)$ is specified in a piecewise manner in eq 26, the wettability contrast does *not* generate discontinuities in $f(\rho)$ across $\rho = \rho_V$. In the following, we consider a *bound* droplet, that is, sufficiently small line tensions, so that the bound state at $\rho = \rho_{bo} > 0$ is the global minimum (see Figure 1). Following this global minimum as a function of the volume or ρ_V (see eq 24) for fixed λ, we find three regimes (see Figure 13).

In regime I, the droplet stays entirely within the domain γ (i.e., $\rho_{bo} < \rho_V$). This is the case for small volumes V_β such that

ρ_V is large. In regime I, the global minimum of f is identical to the local minimum ρ_γ on the γ-domain (i.e., $\rho_{bo} = \rho_\gamma$). The minimum $\rho_\gamma = \rho_\gamma(\rho_V)$ is generally volume- or ρ_V-dependent because of line tension effects. ρ_γ is determined by $\partial_\rho f_\gamma(\rho_\gamma) = 0$ or, equivalently, by the generalized Young equation (eq 20),

$$\cos \theta_\gamma = w_\gamma - \frac{\lambda_V}{\rho_\gamma} = w_\gamma - \lambda \frac{\rho_V}{\rho_\gamma} \qquad (49)$$

which relates ρ_γ to the contact angle $\theta_\gamma = \theta_\gamma(\rho_V)$ of the γ-domain or within regime I, which is also volume-dependent because of line tension effects. ρ_γ and θ_γ also fulfill the geometrical relation in eq 21. Inserting eq 49 into the geometrical relation in eq 21, we obtain self-consistent equations for $\rho_\gamma = \rho_\gamma(\rho_V)$ or the cosine of the contact angle $\cos \theta_\gamma = \cos \theta_\gamma(\rho_V)$.

If we start within regime I and increase the droplet volume to a certain lower boundary volume V_1 corresponding to an upper boundary value $\rho_{V,1}$ and a contact angle $\theta_1 \equiv \theta_\gamma(\rho_{V,1})$, the droplet gets pinned to the boundary, and regime I is left. This happens for $\rho_{bo} = \rho_V$ or $\rho_\gamma(\rho_{V,1}) = \rho_{V,1}$. Then, the Young equation (eq 49) simplifies to an explicit equation for the contact angle θ_1,

$$\cos \theta_1 = w_\gamma - \lambda \qquad (50)$$

and the self-consistent equation for ρ_γ becomes an explicit equation for $\rho_{V,1}$,

$$\rho_{V,1} = \frac{2^{2/3}(1 + w_\gamma - \lambda)^{1/2}}{(1 - w_\gamma + \lambda)^{1/6}(2 + w_\gamma - \lambda)^{1/3}} \qquad (51)$$

In regime III, the droplet spreads onto the surrounding substrate δ and completely covers the γ-domain (i.e., $\rho_{bo} > \rho_V$). This is the case for large volumes V_β such that ρ_V is small. In regime III, the global minimum ρ_{bo} of f is the local minimum ρ_δ of the substrate δ (i.e., $\rho_{bo} = \rho_\delta$). $\rho_\delta = \rho_\delta(\rho_V)$ is again volume- or ρ_V-dependent because of line tension effects and is determined by $\partial_\rho f_\delta(\rho_\delta) = 0$ or the equivalent generalized Young equation (eq 20),

$$\cos \theta_\delta = w_\delta - \frac{\lambda_V}{\rho_\delta} = w_\delta - \lambda \frac{\rho_V}{\rho_\delta} \qquad (52)$$

where $\theta_\delta = \theta_\delta(\rho_V)$ is the volume-dependent contact angle of the δ-substrate or within regime III. Inserting eq 52 into the geometrical relation (eq 21), we also obtain self-consistent equations for $\rho_\delta = \rho_\delta(\rho_V)$ or $\cos \theta_\delta = \cos \theta_\delta(\rho_V)$.

If we start within regime III and decrease the droplet volume to a certain upper boundary volume V_2 corresponding to a lower boundary value $\rho_{V,2}$ and a contact angle $\theta_2 \equiv \theta_\delta(\rho_{V,2})$, the droplet gets pinned to the boundary, and regime III is left. This happens for $\rho_{bo} = \rho_V$ or $\rho_\delta(\rho_{V,2}) = \rho_{V,2}$. Then the Young equation (eq 52) simplifies to an explicit equation for the contact angle θ_2,

$$\cos \theta_2 = w_\delta - \lambda \qquad (53)$$

and the self-consistent equation for ρ_δ gives an explicit equation for $\rho_{V,2}$,

$$\rho_{V,2} = \frac{2^{2/3}(1 + w_\delta - \lambda)^{1/2}}{(1 - w_\delta + \lambda)^{1/6}(2 + w_\delta - \lambda)^{1/3}} \qquad (54)$$

For intermediate volumes $V_1 \leq V \leq V_2$ or $\rho_{V,2} \leq \rho_V \leq \rho_{V,1}$, there is the intermediate regime II, where the contact line is *pinned* at the $\gamma\delta$ domain boundary (the embedding substrate δ
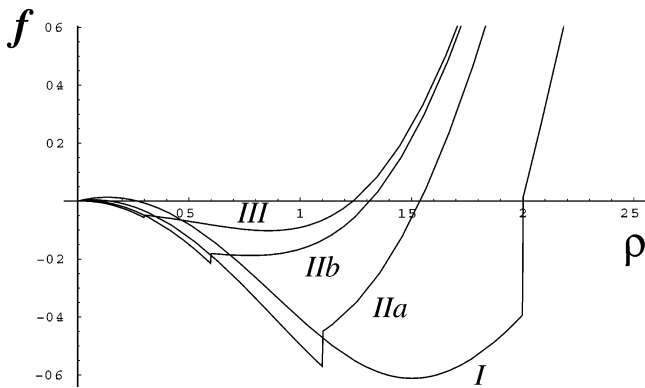
Figure 14. Linophilic domain. Plots of $f(\rho) - f(0)$ according to eq 31, for $w_\gamma = 0.5$, $w_\delta = -0.5$, and $\lambda_\gamma = 0.1$, $\lambda_\delta = 0.2$. Plots from right to left are for $\rho_V = 2.0$, 1.1, 0.6, and 0.3, i.e., for increasing volume corresponding to the four regimes in eq 63. In each of the regimes, $f = f_\gamma$ for $\rho < \rho_V$ and $f = f_\delta$ for $\rho > \rho_V$, according to eq 31. Note the discontinuity in the free energy as given by eq 57.

is lyophobic such that $\rho_{V,2} < \rho_{V,1}$). In this regime II, the global minimum of f is the common *boundary* minimum of f_γ and f_δ at $\rho_{bo} = \rho_V$, and the Young equation, which applies only to *local* minima, is violated. This leads to a freedom of the contact angle in regime II, which varies with the volume in the range $\theta_1 \le \theta \le \theta_2$ according to eq 19,

$$\cos \theta(\rho_V) = \frac{1 - H^2(\rho_V)}{1 + H^2(\rho_V)} \text{ for } \rho_{V,2} \le \rho_V \le \rho_{V,1} \quad (55)$$

Following the global minimum of the free energy (eq 26) at $\rho_{bo} = \rho_{bo}(\rho_V)$ through all three regimes (I−III) by increasing the droplet volume V_β or decreasing ρ_V, we have found

$$\rho_{bo}(\rho_V) = \begin{cases} \rho_\gamma (\rho_V) & \text{for } \rho_V > \rho_{V,1} & \text{regime I} \\ \rho_V & \text{for } \rho_{V,2} \le \rho_V \le \rho_{V,1} & \text{regime II} \\ \rho_\delta (\rho_V) & \text{for } \rho_V < \rho_{V,2} & \text{regime III} \end{cases} \quad (56)$$

where the boundary values fulfill $\rho_\gamma(\rho_{V,1}) = \rho_{V,1}$ and $\rho_\delta(\rho_{V,2}) = \rho_{V,2}$. Thus $\rho_{bo}(\rho_V)$ decreases *continuously* through the pinning and depinning transitions of the contact line at $\rho_V = \rho_{V,1}$ and $\rho_V = \rho_{V,2}$, respectively. The reason for the continuous pinning and depinning transition is that $f(\rho)$ as defined in eq 26 has no discontinuity across $\rho = \rho_V$ such that f_γ and f_δ have a *common* boundary minimum in regime II.

Appendix B. Free Energy Analysis for Circular Lyophilic and Two-Valued Line Tension Contrast

B.1. Line Tension Contrast $\Lambda_\gamma < \Lambda\delta$ (Linophilic Domain). In this appendix, we present the detailed analysis of the free energy $f = f(\rho)$ as given by eq 31 for an axisymmetrical spherical cap-shaped droplet on a circular lyophilic domain in the presence of a line tension contrast, $\Lambda_\gamma < \Lambda_\delta$, which makes the domain linophilic. As opposed to the case of a pure wettability contrast, the piecewise result (eq 31) for the free energy generates a discontinuity Δf of $f(\rho)$ across $\rho = \rho_V$ with

$$\Delta f = f_\delta(\rho_V) - f_\gamma(\rho_V) = \rho_V^2(\lambda_\delta - \lambda_\gamma) \quad (57)$$

which stems from the increase in line free energy upon moving the contact line into the δ-substrate with higher line tension. Similarly to the case of a wettability contrast, we find three distinct regimes when following the global minimum $\rho_{bo} > 0$ of the free energy (eq 31) as a function of the dimensionless surface domain radius ρ_V (see Figure 14).

In regime I, the droplet stays entirely within the domain γ (i.e., $\rho_{bo} < \rho_V$) and evolves as for the case of a homogeneous line tension $\lambda = \lambda_\gamma$, which was treated in Appendix A. The droplet is in regime I for small volumes V_β or large ρ_V. The global minimum of f at ρ_{bo} is identical to the local minimum ρ_γ in the γ-domain, which is determined by $\partial_\rho f_\gamma(\rho_\gamma) = 0$, and the contact angle is θ_γ. As discussed in Appendix A, the volume-dependent local minimum $\rho_\gamma = \rho_\gamma(\rho_V)$ and the cosine of the contact angle $\cos \theta_\gamma = \cos \theta_\gamma(\rho_V)$ can be obtained by combining the relation given in eq 49 (with $\lambda = \lambda_\gamma$) and the geometrical relation given in eq 21.

The boundary volume V_1 or the upper boundary value $\rho_{V,1}$ at which regime I terminates upon increasing the volume are also obtained in the same way as for a homogeneous line tension $\lambda = \lambda_\gamma$. Specifically we find

$$\cos \theta_1 = w_\gamma - \lambda_\gamma \quad (58)$$

for the corresponding contact angle and

$$\rho_{V,1} = \frac{2^{2/3}(1 + w_\gamma - \lambda_\gamma)^{1/2}}{(1 - w_\gamma + \lambda_\gamma)^{1/6}(2 + w_\gamma - \lambda_\gamma)^{1/3}} \quad (59)$$

If the volume is increased such that $\rho_V \le \rho_{V,1}$, the intermediate regime II is reached.

We can also consider a droplet with large volume, which wets the δ-substrate and completely covers the γ-domain and is, thus, in regime III. Then the droplet is in the local minimum $\rho_\delta > \rho_V$ of the δ-substrate, which fulfills $\partial_\rho f_\delta(\rho_\delta) = 0$, and the corresponding contact angle is θ_δ. For large volumes, this state is the global free energy minimum of f. In this state, the droplet behaves as that for the case of a homogeneous line tension $\lambda = \lambda_\delta$, which was treated in Appendix A. As discussed in the previous section, $\rho_\delta = \rho_\delta(\rho_V)$ and the cosine of the contact angle $\cos \theta_\delta = \cos \theta_\delta(\rho_V)$ can be obtained by combining the relation given in eq 52 (with $\lambda = \lambda_\delta$) and the geometrical relation given in eq 21. Upon decreasing the volume, the droplet reaches the $\gamma\delta$ domain boundary for a volume parameter $\rho_{V,2}$ given by the condition $\rho_\delta(\rho_{V,2}) = \rho_{V,2}$. $\rho_{V,2}$ is obtained in the same way as in Appendix A for a homogeneous line tension $\lambda = \lambda_\delta$. Specifically, we find

$$\cos \theta_2 = w_\delta - \lambda_\delta \quad (60)$$

for the corresponding contact angle and

$$\rho_{V,2} = \frac{2^{2/3}(1 + w_\delta - \lambda_\delta)^{1/2}}{(1 - w_\delta + \lambda_\delta)^{1/6}(2 + w_\delta - \lambda_\delta)^{1/3}} \quad (61)$$

The crucial difference compared to the case of a spatially homogeneous line tension lies in the fact that $f(\rho)$ now has a discontinuity across $\rho = \rho_V$ (see Figure 14). For the linophilic domain, this leads to qualitative changes within regimes II and III. For intermediate volumes with $\rho_{V,1} \ge \rho_V \ge \rho_{V,2}$, the global minimum is the boundary minimum of f_γ and $\rho_{bo} = \rho_V$. Therefore, the contact line is *pinned* at the $\gamma\delta$ domain boundary as for a homogeneous line tension; the contact line equation is violated, and the contact angle θ changes with droplet volume according to the above relation (eq 55).

However, the minimum at $\rho = \rho_\delta(\rho_V)$ is no longer the global minimum ρ_{bo} for all larger volumes $V_\beta > V_2$ or $\rho_V < \rho_{V,2}$ because of the discontinuity at $\rho = \rho_V$ (see Figure 14). Increasing the volume starting with V_2 or decreasing ρ_V starting with $\rho_{V,2}$, the minimum ρ_δ appears first as a *metastable* local minimum, while the global minimum is still the boundary minimum of f_γ at ρ_{bo}

$= \rho_V$. Only if this second local minimum becomes the global minimum upon further increasing the volume until V_β is larger than a *critical volume* V_c or ρ_V is smaller than a *critical value* $\rho_{V,c}$ will the contact line finally depin, and we enter regime III, where the droplet spreads onto the substrate δ. At $\rho_V = \rho_{V,c}$, both minima exchange stability such that $\rho_{V,c}$ is determined by the condition $f_\gamma(\rho_{V,c}) = f_\delta(\rho_\delta(\rho_{V,c}))$. Also within the regime $\rho_{V,c} < \rho_V < \rho_{V,2}$, the Young equation is violated, and the contact angle θ changes with droplet volume according to the geometric relation given in eq 19:

$$\cos\theta(\rho_V) = \frac{1 - H^2(\rho_V)}{1 + H^2(\rho_V)} \qquad (62)$$

The same relation determines the critical contact angle θ_c by $\cos\theta_c = \cos\theta(\rho_{V,c})$. Because $\rho_{V,c} < \rho_\delta(\rho_{V,c})$, the global equilibrium radius jumps *discontinuously* from $\rho_{bo} = \rho_{V,c}$ to $\rho_{bo} = \rho_\delta(\rho_{V,c}) > \rho_{V,c}$ at the volume parameter $\rho_V = \rho_{V,c}$. We call the regime $\rho_{V,2} \leq \rho_V \leq \rho_{V,1}$, where the global boundary minimum at $\rho_{bo} = \rho_V$ is the only minimum, regime IIa, and the regime $\rho_{V,c} < \rho_V < \rho_{V,2}$, where an additional metastable minimum at $\rho = \rho_\delta(\rho_V)$ exists, regime IIb.

Within regime III, for $\rho_V < \rho_{V,c}$, the global minimum is the local minimum in the embedding substrate δ, $\rho_{bo} = \rho_\delta$. The contact angle for regime III is the contact angle θ_δ of the substrate δ. Note that, in the entire regime III, the boundary minimum at $\rho = \rho_V$ remains a *metastable* minimum due to the steplike nature of the line tension contrast (eq 29). Therefore, the contact angle in this metastable state can increase dramatically by following the relation given in eq 62 for all $\rho_V \leq \rho_{V,2}$.

Following the global minimum of the free energy (eq 31) at $\rho_{bo} = \rho_{bo}(\rho_V)$ through all three regimes (I–III) by *increasing* the droplet volume V_β or decreasing ρ_V, we find

$$\rho_{bo}(\rho_V) = \begin{cases} \rho_\gamma(\rho_V) & \text{for } \rho_V > \rho_{V,1} & \text{regime I} \\ \rho_V & \text{for } \rho_{V,2} \leq \rho_V \leq \rho_{V,1} & \text{regime IIa} \\ \rho_V & \text{for } \rho_{V,c} < \rho_V < \rho_{V,2} & \text{regime IIb,} \\ & \rho = \rho_\delta(\rho_V) \text{ metastable} \\ \rho_\delta(\rho_V) & \text{for } \rho_V < \rho_{V,c} & \text{regime III,} \\ & \rho = \rho_V \text{ metastable} \end{cases}$$

$$(63)$$

Whereas $\rho_{bo}(\rho_V)$ changes *continuously* upon pinning of the contact line at $\rho_V = \rho_{V,1}$ between regimes I and II, there is a *discontinuous depinning transition* of the contact line between regimes II and III at $\rho_V = \rho_{V,c}$, which is caused by the line tension contrast. The corresponding morphological diagram, as discussed in 5.1, is shown in Figure 6 (for $\Delta\lambda = \lambda_\delta - \lambda_\gamma > 0$). Calculating the global minima $f(\rho_{bo}(\rho_V))$ of the free energy and the metastable free energy minima as a function of ρ_V, we obtain the corresponding bifurcation diagram in Figure 7 and observe the strong hysteretic effect mentioned in section 5.1. In the bifurcation diagram in Figure 7, we also complete the Gibbs triangle of the discontinuous transition by plotting the unstable boundary maximum $f_\delta(\rho_V)$ for $\rho_V < \rho_{V,2}$.

B.2. Line Tension Contrast $\Lambda_\gamma > \Lambda_\delta$ (Linophobic Domain). In this appendix, we present the detailed analysis of the free energy $f = f(\rho)$ as given by eq 31 for an axisymmetrical spherical cap-shaped droplet on a circular lyophilic domain in the presence of a line tension contrast $\Lambda_\gamma > \Lambda_\delta$, which makes the domain linophobic.

The depinning behavior for the case in which $\Lambda_\gamma < \Lambda_\delta$ for *increasing* volume treated in the previous section will be similar
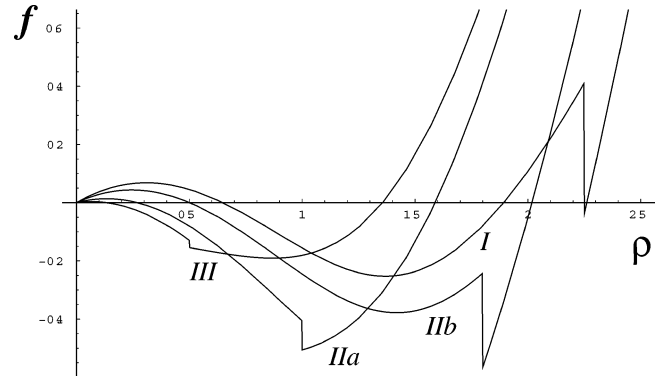

Figure 15. Linophobic domain. Plots of $f(\rho) - f(0)$ according to eq 31, for $w_\gamma = 0.5$, $w_\delta = -0.5$, and $\lambda_\gamma = 0.2$, $\lambda_\delta = 0.1$. Plots from right to left are for $\rho_V = 2.25$, 1.8, 1, and 0.5, i.e., for increasing volume corresponding to the four regimes in eq 64.

to the depinning behavior for $\Lambda_\gamma > \Lambda_\delta$ for *decreasing* volume. In both cases, the contact line depins discontinuously from the boundary of the circular domain upon entering into the region with the less favorable line tension.

In regime III, the droplet wets the surrounding substrate δ and completely covers the γ-domain (i.e., $\rho_{bo} > \rho_V$). In this regime, it evolves as for the case of a homogeneous line tension $\lambda = \lambda_\delta$, treated in Appendix A. The droplet is in regime III for large volumes V_β or small ρ_V. The global minimum of f at ρ_{bo} is the local minimum ρ_δ on the δ-substrate, which is determined by $\partial_\rho f_\delta(\rho_\delta) = 0$, and the contact angle is θ_δ. As discussed in Appendix A, the volume-dependent local minimum $\rho_\delta = \rho_\delta(\rho_V)$ and the cosine of the contact angle $\cos\theta_\delta = \cos\theta_\delta(\rho_V)$ can be obtained by combining the relation in eq 52 (with $\lambda = \lambda_\delta$) and the geometrical relation in eq 21.

The boundary volume V_2 or the lower boundary value $\rho_{V,2}$ at which regime III terminates upon decreasing the volume are also obtained in the same way as for a homogeneous line tension, $\lambda = \lambda_\delta$. For $\rho_{V,2}$ and the corresponding contact angle θ_2, we obtain the same equations (61 and 60) as for the linophilic case. If the volume is decreased such that $\rho_V \geq \rho_{V,2}$, the intermediate regime II is reached.

We can also consider a droplet with small volume V_β, which stays within the γ-domain. Then the droplet is in the local minimum $\rho_\gamma < \rho_V$ of the γ-domain, which fulfills $\partial_\rho f_\gamma(\rho_\gamma) = 0$, and the corresponding contact angle is θ_γ. In this state, the droplet behaves as for the case of a homogeneous line tension, $\lambda = \lambda_\gamma$, which was treated in the Appendix A. As discussed there, $\rho_\gamma = \rho_\gamma(\rho_V)$ and the cosine of the contact angle $\cos\theta_\gamma = \cos\theta_\gamma(\rho_V)$ can be obtained by combining the relation given in eq 49 (with $\lambda = \lambda_\gamma$) and the geometrical relation given in eq 21. Upon increasing the volume, the droplet reaches the $\gamma\delta$ domain boundary for a volume parameter $\rho_{V,1}$ given by the condition $\rho_\gamma(\rho_{V,1}) = \rho_{V,1}$. $\rho_{V,1}$ is obtained in the same way as described in Appendix A for a homogeneous line tension, $\lambda = \lambda_\gamma$. For $\rho_{V,1}$ and the corresponding contact angle θ_1, we obtain the same equations (59 and 58) as for the linophilic case.

Also, for the linophobic case, the crucial difference to the case of a spatially homogeneous line tension is the discontinuity of $f(\rho)$ across $\rho = \rho_V$ (see Figure 15. For the linophobic domain, this leads to qualitative changes within regimes I and II. For intermediate volumes with $\rho_{V,1} \geq \rho_V \geq \rho_{V,2}$, the global minimum is the boundary minimum of f_δ and $\rho_{bo} = \rho_V$. Therefore, the contact line is *pinned* at the $\gamma\delta$ domain boundary as for a homogeneous line tension; the contact line equation is violated, and the contact angle θ changes with droplet volume according to the above relation (eq 55).

However, the minimum at $\rho = \rho_\gamma(\rho_V)$ is no longer the global minimum ρ_{bo} for all smaller volumes $V_\beta < V_1$ or $\rho_V > \rho_{V,1}$ due to the discontinuity at $\rho = \rho_V$ (see Figure 15). Decreasing the volume starting with V_1 or increasing ρ_V starting with $\rho_{V,1}$, the minimum ρ_γ appears first as a *metastable* local minimum, while the global minimum is still the boundary minimum of f_δ at $\rho_{bo} = \rho_V$. Only if this second local minimum becomes the global minimum upon further increasing the volume until V is larger than a *critical volume* V_c^* or ρ_V is smaller than a *critical value* $\rho_{V,c}^*$ will the contact line finally depin, and we enter regime I, where the droplet retreats to the domain γ. At $\rho_V = \rho_{V,c}^*$, both minima exchange stability such that $\rho_{V,c}^*$ is determined by the condition $f_\delta(\rho_{V,c}^*) = f_\gamma(\rho_\gamma(\rho_{V,c}^*))$. Also, within the regime $\rho_{V,1} < \rho_V < \rho_{V,c}^*$, the Young equation is violated, and the contact angle θ changes with droplet volume according to the geometric relation given in eq 62, which also determines the critical contact angle θ_c^* by $\cos \theta_c^* = \cos \theta(\rho_{V,c}^*)$. Because $\rho_{V,c}^* > \rho_\gamma(\rho_{V,c}^*)$, the global equilibrium radius jumps *discontinuously* from $\rho_{bo} = \rho_{V,c}^*$ to $\rho_{bo} = \rho_\gamma(\rho_{V,c}^*) < \rho_{V,c}^*$ at the volume parameter $\rho_V = \rho_{V,c}^*$. We call the regime $\rho_{V,2} \le \rho_V \le \rho_{V,1}$, where the global boundary minimum at $\rho_{bo} = \rho_V$ is the only minimum, regime IIa, and the regime $\rho_{V,1} < \rho_V < \rho_{V,c}^*$, where an additional metastable minimum at $\rho = \rho_\gamma(\rho_V)$ exists, regime IIb.

Within regime I, for $\rho_V > \rho_{V,c}^*$, the global minimum is the local minimum of the domain γ, $\rho_{bo} = \rho_\gamma$. The contact angle for regime I is the contact angle θ_γ of the substrate γ. Note that, in the entire regime I, the boundary minimum at $\rho = \rho_V$ remains a *metastable* minimum due to the steplike nature of the line tension contrast (eq 29). Therefore, the contact angle in this metastable state can decrease dramatically by following the relation given in eq 62 for $\rho_V \ge \rho_{V,1}$.

Following the global minimum of eq 31 as a function of ρ_V (i.e., $\rho_{bo} = \rho_{bo}(\rho_V)$) through all three regimes (III−I) by *decreasing* the droplet volume V_β or increasing ρ_V, we find

$$\rho_{bo}(\rho_V) = \begin{cases} \rho_\delta(\rho_V) & \text{for } \rho_V < \rho_{V,2} & \text{regime III} \\ \rho_V & \text{for } \rho_{V,2} \le \rho_V < \rho_{V,1} & \text{regime IIa} \\ \rho_V & \text{for } \rho_{V,1} \le \rho_V < \rho_{V,c}^* & \text{regime IIb,} \\ & \rho = \rho_\gamma(\rho_V) \text{ metastable} \\ \rho_\gamma(\rho_V) & \text{for } \rho_V > \rho_{V,c}^* & \text{regime I,} \\ & \rho = \rho_V \text{ metastable} \end{cases} \tag{64}$$

Thus, $\rho_{bo}(\rho_V)$ changes *continuously* at the pinning of the contact line at $\rho_V = \rho_{V,2}$ between regimes III and II, but there is a *discontinuous depinning transition* of the contact line between regimes II and I at $\rho_V = \rho_{V,c}^*$, which is caused by the line tension contrast. Figure 6 shows the corresponding morphological diagram (for $\Delta\lambda = \lambda_\delta - \lambda_\gamma < 0$), and Figure 8 shows the corresponding bifurcation diagram of the global and metastable free energy minima, as previously discussed in section 5.1. In the bifurcation diagram in Figure 8, we also complete the Gibbs triangle of the discontinuous transition by plotting the unstable boundary maximum $f_\gamma(\rho_V)$ for $\rho_V > \rho_{V,1}$.

B.3. Contact Radius and Contact Angle Discontinuities at Depinning. In this appendix, we calculate the discontinuities in droplet contact radius and contact angle at the discontinuous depinning transitions.

For a linophilic domain ($\Lambda_\gamma < \Lambda_\delta$), the size of the discontinuity $\Delta\rho_{bo} \equiv \rho_\delta(\rho_{V,c}) - \rho_{V,c} > 0$ in the dimensionless droplet radius at the depinning transition from regime IIb to regime III can be calculated from the two conditions $f_\gamma(\rho_{V,c}) = f_\delta(\rho_\delta)$ and $\partial_\rho f_\delta(\rho_\delta) = 0$ for $\rho_{V,c}$ and ρ_δ. Assuming that $\Delta\rho_{bo} \ll 1$ is small, we expand

$f_\delta(\rho)$ around $\rho_{V,c}$ and obtain the conditions

$$f_\gamma(\rho_{V,c}) = f_\delta(\rho_\delta) \approx f_\delta(\rho_{V,c}) + \Delta\rho_{bo}\partial_\rho f_\delta(\rho_{V,c})$$

$$0 = \partial_\rho f_\delta(\rho_\delta) \approx \partial_\rho f_\delta(\rho_{V,c}) + \Delta\rho_{bo}\partial_\rho^2 f_\delta(\rho_\delta) \tag{65}$$

which can be combined into the result

$$\Delta\rho_{bo}^2 \approx \frac{f_\delta(\rho_{V,c}) - f_\gamma(\rho_{V,c})}{\partial_\rho^2 f_\delta(\rho_{V,c})} \approx \frac{\Delta f}{\partial_\rho^2 f_\delta(\rho_\delta)} \tag{66}$$

Using the result from eq 18 for $\partial_\rho^2 f_\delta$ together with the relation

$$H^2(\rho_\delta) = \frac{1 - \cos\theta_\delta}{1 + \cos\theta_\delta} \tag{67}$$

and neglecting line tension contributions in the contact line equation, we can write

$$\partial_\rho^2 f_\delta(\rho_\delta) \approx (1 - w_\delta)(2 + 3w_\delta + w_\delta^2) \tag{68}$$

in terms of the wettability of the δ-substrate. Using eq 57 for the free energy discontinuity Δf, we arrive at our final result

$$\Delta\rho_{bo} \approx \rho_{V,c}\left[\frac{\lambda_\delta - \lambda_\gamma}{(1 - w_\delta)(2 + 3w_\delta + w_\delta^2)}\right]^{1/2} \tag{69}$$

Thus the discontinuity $\Delta\rho_{bo}$ at the discontinuous depinning transition of the contact line depends on (i) the critical droplet volume, (ii) the line tension contrast, and (iii) the wettability or contact angle of the δ-substrate.

We can use the result from eq 69 to obtain the discontinuity in the contact angle $\Delta\theta \equiv \theta_\delta - \theta_c < 0$ by expanding the relation given in eq 19 for $\cos\theta$,

$$\Delta\theta \approx -\frac{1}{\sin\theta_\delta}\frac{\Delta\rho_{bo}}{\rho_\delta}\frac{4H^2(\rho_\delta)(3 + H^2(\rho_\delta))}{(1 + H^2(\rho_\delta))^3}$$

$$\approx -2^{1/6}\rho_{V,c}(\lambda_\delta - \lambda_\gamma)^{1/2}(1 - w_\delta)^{2/3}(2 + w_\delta)^{5/6} \tag{70}$$

where we neglected line tension contributions in the contact line equation.

For a linophobic domain ($\Lambda_\gamma > \Lambda_\delta$), the calculation of the discontinuities $\Delta\rho_{bo}^* \equiv \rho_\gamma(\rho_{V,c}^*) - \rho_{V,c}^* < 0$ in the dimensionless radius and $\Delta\theta^* \equiv \theta_\gamma - \theta_c^* > 0$ in the contact angle at the depinning transition of the contact line from regime IIb to regime I proceeds analogously with the result

$$\Delta\rho_{bo}^* \approx -\rho_{V,c}^*\left[\frac{\lambda_\gamma - \lambda_\delta}{(1 - w_\gamma)(2 + 3w_\gamma + w_\gamma^2)}\right]^{1/2}$$

$$\Delta\theta^* \approx 2^{1/6}\rho_{V,c}^*(\lambda_\delta - \lambda_\gamma)^{1/2}(1 - w_\gamma)^{2/3}(2 + w_\gamma)^{5/6} \tag{71}$$

Appendix C: List of Symbols

α	vapor phase
a	radius of the circular domain
$A_{\alpha\beta}$	area of the liquid−vapor interface
$\mathcal{A}_{\alpha\beta}$	surface of the liquid−vapor interface
$\mathcal{A}_{\beta\sigma}$	surface of the liquid−solid interface
$\mathcal{A}_{\mathcal{H}}$	Hamaker constant
β	liquid phase
c_g^*	geodesic curvature of the contact line

δ	lyophobic substrate
Δf	discontinuity in f at $\rho = \rho_V$
$\Delta \lambda$	dimensionless line tension contrast
ΔP	Laplace pressure
$\Delta \rho_{bo}$, $\Delta \rho_{bo}^*$	discontinuity of ρ at depinning
$\Delta \theta$, $\Delta \theta^*$	discontinuity of θ at depinning
f	dimensionless free energy
f_δ	f in the lyophobic matrix
f_γ	f in the lyophilic domain
γ	lyophilic substrate
h	maximal height of the droplet
H	dimensionless maximum height of the droplet (eq 12)
k_B	Boltzmann constant
l	droplet profile in interface model
L_β	linear size of the droplet (eq 11)
L_β^*	characteristic length scale (eq 6)
$\ell_{\alpha\beta}$	liquid−vapor interface width
$\ell_{\alpha\beta\gamma}$	contact line width
$\bar{\ell}_{\alpha\beta\gamma}$	dimensionless contact line width
$\mathscr{L}_{\alpha\beta\gamma}$	three-phase contact line
ℓ_G	capillary length
l_{min}	interface position minimizing $U(l)$
ℓ_{mol}	typical intermolecular distance
l_{pin}	inflection point of $U(l)$
λ_V	dimensionless volume-dependent line tension (eq 12)
λ	dimensionless volume-independent line tension (eq 25)
λ_γ	λ in the γ-domain
λ_δ	λ on the δ-substrate
$\lambda_{V,in}$	instability threshold of λ (eq 23)
$\lambda_{V,ub}$	unbinding threshold of λ (eq 22)
Λ	line tension
$\Lambda_{V,\delta}$	Λ in the lyophobic domain
$\Lambda_{V,\gamma}$	Λ in the lyophilic domain
Λ_{vdW}	contribution to Λ from van der Waals forces
$\hat{\mathbf{m}}$	conormal of the contact line
M	mean curvature of the droplet
P_α	pressure of the vapor phase
P_β	pressure of the liquid phase
r	radius of the contact area of a spherical droplet
R	curvature radius of a spherical droplet
R_1, R_2	lower/upper boundary curvature radii at pinning
ρ	dimensionless radius of contact area (eq 12)
ρ_V	dimensionless domain radius (eq 24)
$\rho_{V,1}, \rho_{V,2}$	upper/lower boundary values of ρ_V
$\rho_{V,c}$	critical ρ_V (linophilic domain)
$\rho_{V,c}^*$	critical ρ_V (linophobic domain)
ρ_{bo}	equilibrium value of ρ (bound droplet)
ρ_{eff}	effective ρ of contact area (eq 46)
σ	solid substrate
$\Sigma_{\alpha\beta}$	interfacial energy of the liquid−vapor interface
$\Sigma_{\alpha\sigma}$	interfacial energy of vapor−substrate interface
$\Sigma_{\beta\sigma}$	interfacial energy of liquid−substrate interface
T	temperature
θ	contact angle
θ_1, θ_2	lower/upper boundary values of θ at pinning
θ_∞	θ of a macroscopic droplet
θ_δ	θ on the lyophobic matrix
$\theta_{\delta,\infty}$	θ_∞ on the lyophobic matrix
θ_γ	θ on the lyophilic domain
$\theta_{\gamma,\infty}$	θ_∞ on the lyophilic domain
θ_c, θ_c^*	critical θ
$\Theta(x)$	Heaviside function
$U(l)$	attractive interface potential
U_{min}	minimum of $U(l)$
V_1, V_2	lower/upper boundary volumes
V_c, V_c^*	critical volume
V_β	volume of the droplet
$w(x)$	local wettability (eq 4)
w_δ	w of the lyophobic matrix
w_γ	w of the lyophilic domain
w_{in}	instability threshold of w
w_{ub}	unbinding threshold of w
$\mathbf{x}$	coordinate on the substrate